Surface ozone-meteorology relationships: Spatial variations and the role of the jet stream

Gaige Hunter Kerr[1], Darryn W. Waugh[2,3], Stephen D. Steenrod[3,4], Sarah A. Strode[3,4], and Susan E. Strahan[3,4]

[1]Department of Earth and Planetary Sciences, Johns Hopkins University, Baltimore, Maryland, USA
[2]School of Mathematics and Statistics, University of New South Wales, Sydney, New South Wales, Australia
[3]NASA Goddard Space Flight Center, Greenbelt, Maryland, USA
[4]Universities Space Research Association, GESTAR, Columbia, Maryland, USA

Key Points:

- Positive relationships among O_3, temperature, and humidity hold only in the continental mid-latitudes
- These relationships stem from the association of O_3 with meteorology, not chemistry or emissions
- The jet stream position affects heat, moisture, and O_3 transport by altering the mean meridional flow

Corresponding author: G. H. Kerr, `gaige.kerr@jhu.edu`

Abstract

We investigate the relationships among summertime ozone (O_3), temperature, and humidity on daily timescales across the Northern Hemisphere using observations and model simulations. Temperature and humidity are significantly positively correlated with O_3 across continental regions in the mid-latitudes ($\sim 35-60°$N), but this is not the case at high latitudes, in the subtropics, and over the oceans. These O_3-meteorology relationships are due to an indirect association with transport rather than through the direct dependence of chemistry or emissions, and their spatial patterns are linked to the position and meridional movement of the jet stream. Within the latitudinal range of the jet, there is an increase (decrease) in O_3, temperature, and humidity over land with poleward (equatorward) movement of the jet, while over the oceans poleward movement of the jet results in decreases of these fields and vice versa. Beyond the latitudes where the jet traverses, the meridional movement of the jet stream has variable or negligible effects on surface-level O_3, temperature, and humidity. The movement of the jet influences these fields primarily by altering the surface-level meridional flow, and the O_3-meteorology relationships are largely the product of the jet-induced changes in the surface-level transport by the mean meridional circulation. These results underscore the importance of considering the role of the jet stream and the mean meridional circulation for the O_3-meteorology relationships, especially in light of expected changes to these features under climate change.

Plain Language Summary

There is no uniform relationship of ozone (O_3) with meteorological variables such as temperature and humidity at the earth's surface across the Northern Hemisphere. However, in the mid-latitudes over land, higher temperature and humidity are generally associated with higher concentrations of O_3, but this is not the case elsewhere. We use detailed computer simulations of atmospheric chemistry to show that these relationships are the result of changes in meteorology, not changes in emissions or chemistry. The relationships between O_3 and meteorological variables are related to the north-south movement of the "jet stream," powerful eastward-flowing air currents located > 5 km aloft in the atmosphere that can encircle the hemisphere. Specifically, we find that the jet stream influences the O_3-meteorology relationships due to its effect on north- and southward fluxes of O_3, heat, and moisture and not due to storm systems, as has been previously suggested. Our results are relevant for understanding the present-day O_3-meteorology relationships and how climate change may impact O_3 pollution.

1 Introduction

Ambient surface-level ozone (O_3) plays a prominent role in atmospheric chemistry (Fiore et al., 2015; Pusede et al., 2015) and the climate system (Tarasick et al., 2019), while posing significant threats to human health (Landrigan et al., 2018) and ecosystem productivity (Tai & Martin, 2017). Long-term trends in observed O_3 in the Northern Hemisphere mid-latitudes reveal sustained, year-round increases in baseline O_3 concentrations (Parrish et al., 2012), underpinning the need for a better understanding of the drivers of O_3 variability. Meteorology strongly affects O_3 concentrations and chemistry through both variations in prevailing weather conditions on daily, seasonal, or interannual timescales as well as long-terms trends associated with climate change (e.g., Jacob & Winner, 2009; Fiore et al., 2015; Otero et al., 2016; Lefohn et al., 2018). However, the meteorological phenomena that affect O_3 are not direct relationships in the same sense as emissions or kinetics and energetics. Previous studies have focused on characterizing the relationship between O_3 and temperature or humidity in historical data. Generally these studies found a positive O_3-temperature relationship (e.g., Rasmussen et al., 2012, 2013; Pusede et al., 2015) and a variable O_3-humidity relationship with substantial latitudinal variability (e.g., Camalier et al., 2007; Tawfik & Steiner, 2013; Kavassalis & Murphy, 2017).

The majority of past studies on the O_3-meteorology relationships focused on populated, industrialized portions of the Northern Hemisphere mid-latitudes, potentially overlooking important variations of these relationships elsewhere. These studies have been conducted for different and often non-overlapping time periods during which changes of O_3 precursors could affect chemical background conditions (Kim et al., 2006; Derwent et al., 2010; Cooper et al., 2012; Simon et al., 2015; Lin et al., 2017). Finally, past studies have used different methodologies (e.g., O_3-relationships derived from hourly, daily, or seasonal data; see Brown-Steiner et al. (2015) for additional information). All these factors complicate direct comparisons from study to study; thus, it is difficult to piece together a comprehensive sense of how the O_3-meteorology relationships vary across the globe and what processes drive these relationships. Recent work by Kerr et al. (2019) and Porter and Heald (2019) suggests that greater than 50% of the covariance of O_3 and temperature in the United States (U.S.) and Europe on daily timescales stems from meteorological phenomena, not chemistry or emissions. It is an open question whether this also holds for the O_3-humidity relationship.

There have been several meteorological, or transport-related, mechanisms proposed to link O_3 with temperature or humidity. However, little consensus exists as to which mechanism is the most important in linking temperature and humidity with O_3 and the regions or timescales over which it operates. Baroclinic cyclones can disperse built-up concentrations of pollution by entraining polluted air from the planetary boundary layer (PBL) into the free troposphere (Mickley, 2004; Leibensperger et al., 2008; Knowland et al., 2015, 2017). Quasi-stationary anticyclones such as the Bermuda High can influence regional climate and O_3 (e.g., Zhu & Liang, 2013). Properties of the PBL, such as its height or temperature inversions and mixing within the PBL, have also been suggested as transport-related mechanisms that affect surface-level O_3 (Dawson et al., 2007; He et al., 2013; Reddy & Pfister, 2016; Barrett et al., 2019). Winds near the earth's surface or aloft can ventilate pollution away from its source region (Camalier et al., 2007; Hegarty et al., 2007; Tai et al., 2010; Sun et al., 2017). Interactions among the atmosphere, land surface, and biosphere have been proposed to explain the O_3-humidity relationship in North America (Tawfik & Steiner, 2013; Kavassalis & Murphy, 2017). The jet stream is a pronounced feature of the general circulation of atmosphere in both the Northern and Southern Hemisphere mid-latitudes and is characterized by a region of strong eastward wind aloft. Its existence arises from momentum and heat fluxes forced by transient eddies, and the jet extends throughout the depth of the troposphere (Woollings et al., 2010). The variability of surface-level summertime O_3 as well as its relationship with temperature have been linked to the latitude of the jet stream over eastern North America (Barnes & Fiore, 2013; Shen et al., 2015). Similar connections between the jet position, persistence of the jet in a given position, and wintertime particulate matter with a diameter $< 2.5\ \mu$m ($PM_{2.5}$) have also been demonstrated in Europe (Ordóñez et al., 2019).

The aim of this paper is to document the relationships of surface-level temperature and specific humidity (henceforth "humidity") with O_3 in the Northern Hemisphere during boreal summer and explore the processes responsible for spatial variations of these relationships. Through our model simulations, we demonstrate that transport-related processes, not chemistry or emissions, drive the covariance of O_3 with temperature and humidity. We build off of the previous regionally-focused work of Barnes and Fiore (2013), Shen et al. (2015), and Ordóñez et al. (2019) to show the connections between the position of the jet stream and surface-level temperature, humidity, and O_3 variability hold across the Northern Hemisphere. Finally, we develop and test hypotheses that tie the jet stream to the surface-level relationships among O_3, temperature, and humidity.

2 Data and Methodology

2.1 Model Simulations

The majority of our analysis of the O_3-meteorology relationships is performed using simulations of NASA's Global Modeling Initiative chemical transport model (GMI CTM; Duncan et al., 2007; Strahan et al., 2007, 2013). The GMI CTM is driven by meteorological fields from the Modern-Era Retrospective analysis for Research and Applications, version 2 (MERRA-2; Gelaro et al., 2017). GMI CTM simulations used in this study have 1° latitude x 1.25° longitude horizontal resolution ($\sim$ 100 km) with 72 vertical levels, extending from the surface to 0.01 hPa. The chemical mechanism of the CTM includes tropospheric and stratospheric chemistry with approximately 120 species and over 400 reactions. Information about the natural and anthropogenic emission inventories and model parameterizations (e.g., biogenic emissions, lightning NO_x, etc.) for the current model configuration is provided in Kerr et al. (2019).

The GMI CTM is a proven model to understand surface-level O_3 variability and its drivers (e.g., Duncan et al., 2008; Strode et al., 2015; Kerr et al., 2019). Kerr et al. (2019) evaluated the CTM with observations from *in-situ* networks in the U.S. and showed that the model skillfully simulated the observed summertime variability of O_3 during the afternoon despite a high model bias in the eastern U.S. and low model bias in the western U.S; these biases are common among CTMs (e.g., Brown-Steiner et al., 2015; Guo et al., 2018; Phalitnonkiat et al., 2018).

In this study we focus on the O_3-meteorology relationships in the Northern Hemisphere for a three-year period (2008−2010) during boreal summer (1 June−31 August). We use O_3 from the model's surface level, which has a nominal thickness of $\sim$ 130 m. CTM output from the early afternoon (mean 1300 − 1400 local time), coinciding with the overpass time of the Afternoon Constellation ("A-Train") of Earth observing satellites, was archived as gridded fields, whereas hourly output was archived only at select sites. We consequently use modeled O_3 from this early afternoon period, noting that this time of day typically represents a time in which the PBL is well-mixed (Cooper et al., 2012) and daily O_3 concentrations reach their maximum (Schnell et al., 2014). Considering O_3 during this early afternoon period versus longer averaging periods leads to similar results (Kerr et al., 2019).

Two simulations are analyzed in this study. The first is a control simulation with daily (or sub-daily) variations in meteorological inputs, chemistry, and natural emissions. Anthropogenic emissions in this simulation vary from month to month. Unless otherwise indicated, all subsequent figures and analysis use this control simulation. In a second simulation referred to as "transport-only," we isolate the role of transport. Fields that affect chemistry (e.g., temperature, clouds and albedo-related variables, surface roughness, specific humidity, and ground wetness) are averaged such that their diurnal cycles are identical for all days within a month for a particular grid cell. Natural and anthropogenic emissions are fixed to monthly mean values. Only the diurnal variations of wind, precipitation, convective mass flux, pressure, and PBL height change from day to day in this simulation. This transport-only simulation is similar to the "Transport" simulation discussed in Kerr et al. (2019) with the exception that specific humidity is also averaged to a monthly mean diurnal cycle.

2.2 Observations

We use *in-situ* observations of O_3 across North America, Europe, and China to examine the observed variations of the O_3-meteorology relationships and assess the accuracy of the GMI CTM. We choose these regions because their *in-situ* networks, described below, measure and archive O_3 hourly. Since the model outputs O_3 averaged over 1300-1400 hours (local time), comparing this output with hourly O_3 observations averaged over the same time of the day represents the most direct comparison. The lack of *in-situ* networks with observations at a high temporal frequency in many other parts of the world hinders our ability to examine model performance over other regions.

Observations of O_3 from 233 Canadian sites are part of the National Air Pollution Surveillance Network (NAPS), collected and analyzed by Environment and Climate Change Canada (ECCC, 2017). In the U.S. we use observations from the Air Quality System (AQS), which contains O_3 observations collected by the U.S. Environmental Protection Agency and state, local, and tribal air pollution control agencies at 1483 sites (EPA, 2019). The European Monitoring and Evaluation Programme (EMEP) provides O_3 observations at 142 sites in the European Union (Hjellbrekke & Solberg, 2019).

For China we use observations from the Chinese Ministry of Ecology and Environment (MEE) for summers 2016−2017 (Li et al., 2019). Observations are primarily from urban centers, and if a particular Chinese city has > 1 monitor, a city-wide average was computed following Z. Zhao and Wang (2017), resulting in data from 360 Chinese cities. The choice of this $2016 - 2017$ time period is because this Chinese observational network did not come online until the mid-2010s. Accordingly, when we assess the performance of the GMI CTM and discuss the observed O_3-meteorology relationships in China, we use model simulations (Section 2.1) and reanalysis data (Section 2.3) for 2016−2017 rather than the $2008 - 2010$ period used elsewhere in this study.

2.3 Meteorological Reanalysis

In addition to providing meteorological input to drive the GMI CTM, MERRA-2 is also used to determine the relationships between O_3 and meteorology. Several of the observational networks detailed in Section 2.2 lack co-located meteorological observations, and Varotsos et al. (2013) commented that lack of co-located O_3 and temperature (or other meteorological) observations necessitates the use of gridded products to examine the relationships between O_3 and meteorology.

MERRA-2 meteorological fields are not available at the satellite overpass times sampled by the GMI CTM simulations (Section 2.1). We calculate daily averages from the following MERRA-2 fields: hourly 10-m zonal (U_{10}) and meridional (V_{10}) wind, three-hourly 2-m specific humidity (q), three-hourly 500 hPa zonal wind (U_{500}), and hourly PBL height ($PBLH$). Daily 2-m maximum temperature (T) is computed as the maximum of hourly values. Our use of daily maximum temperature follows Zhang and Wang (2016) and Meehl et al. (2018).

There are uncertainties associated with an assimilated product like MERRA-2, but Bosilovich et al. (2015) presented evidence that MERRA-2 provides a very good quality reanalysis data set. As the MERRA-2 data have higher horizontal resolution than the GMI CTM (0.5° latitude ×0.625° longitude for MERRA-2 versus 1° latitude ×1.25° longitude for the CTM), we degrade the MERRA-2 data to the resolution of the CTM using xESMF, a universal regridding tool for geospatial data (Zhuang, 2018).

2.4 Methodology

2.4.1 Statistical analysis

We use the Pearson product-moment correlation coefficient and the slope of the ordinary least squares (OLS) regression (denoted $r(x, y)$ and dy/dx for variables x and y, respectively) to (1) quantify the O_3-meteorology relationships on daily timescales and (2) evaluate the ability of the GMI CTM to accurately simulate observed O_3 from the *in-situ* networks detailed in Section 2.2. The correlation coefficient is a parametric test that measures the degree of linear correlation between x and y, and the OLS regression describes the linear relationship between x (explanatory variable) and y (dependent variable).

The serial dependence (persistence) in our meteorological and chemical data reduces the effective sample size by an amount not known *a priori* and inhibits the use of traditional hypothesis testing methods such as t-tests to evaluate significance (Zwiers & von Storch, 1995; Wilks, 1997; Mudelsee, 2003). Therefore, we use moving block bootstrapping to quantify the significance of the correlation coefficient. While traditional bootstrapping resamples individual, independent values of the time series, moving block bootstrapping resamples continuous subsets of the time series with blocklength L and does not destroy the ordering responsible for the persistence (Wilks, 2011). At each grid cell we synthetically construct a null distribution of 10000 bootstrapped realizations of the correlation coefficient (Mudelsee, 2014) and use $L = 10$ days. As a rule of thumb, blocklengths should generally exceed the decorrelation time. More rigorous methods for optimizing L exist, but we find that $L = 10$ is adequate for our application and our results are not sensitive to the exact value of L. To evaluate the significance, we estimate the 95% confidence interval using the percentile method of the bootstrapped values (i.e., the 95% confidence interval of our 10000 realizations is given by the 250th and 9750th sorted values). If this confidence interval does not contain zero, we declare the correlation coefficient significant.

2.4.2 Jet stream position

We define the latitude of the jet (ϕ_{jet}) as the latitude of maximum zonal winds at 500 hPa (U_{500}) on each day. This approach to determine ϕ_{jet} follows Barnes and Fiore (2013) but differs in two ways: (1) Barnes and Fiore (2013) determined using U_{500} averaged over the eastern North America zonal sector. We determine ϕ_{jet} locally (at each longitudinal grid cell) and between 20$-$70°N; (2) After finding the maximum U_{500} for each longitude, we employ a simple moving average that is essentially a convolution of daily ϕ_{jet} of a general rectangular pulse with width $\sim 10°$. We also conducted similar analyses with unsmoothed data and by varying the width of the pulse and obtained similar results.

2.4.3 Cyclone detection and tracking

To assess the impact of extratropical cyclones on surface-level O_3, we use the MAP Climatology of Mid-latitude Storminess (MCMS) database to locate cyclones (Bauer & Genio, 2006; Bauer et al., 2016). Within MCMS, cyclones are detected as minima in the ERA-Interim sea level pressure (SLP) dataset (Dee et al., 2011) and are subject to additional filters to screen for spurious detections. Once detected, MCMS tracks cyclones with criteria that require gradual changes in SLP, no sudden changes in direction, and cyclones travel distances < 720 km over single six-hourly time steps. Additional details can be found in Bauer and Genio (2006) and Bauer et al. (2016).

3 Global O_3 distribution and evaluation

We begin with an analysis of the distribution and variability of modeled surface-level O_3 during summer (Figure 1a). Concentrations of O_3 are highest ($\sim 35-60$ ppbv) in a broad mid-latitude band over continental regions extending from $20-50°$N. The GMI CTM suggests that O_3 is not zonally-symmetric within this mid-latitude band and that the highest mean concentrations (> 50 ppbv) are in the Middle East and central and eastern Asia. Outside of the mid-latitudes, the CTM simulates lower O_3 concentrations ($<$ 30 ppbv), and the lowest concentrations in the hemisphere ($<$ 15 ppbv) are found in the remote tropical marine atmosphere. This spatial distribution of mean summertime surface O_3 is consistent with other models (e.g., Sadiq et al., 2017). We characterize the daily variability of O_3 by the standard deviation, and two levels (8 and 10 ppbv) are highlighted with the thin dashed and thick contours in Figure 1a.

To illustrate the possible influence of anthropogenic emissions on the spatial variability of mean O_3 concentrations, we show mean annual anthropogenic NO_x emission data from the Emissions Database for Global Atmospheric Research (EDGAR; Crippa et al., 2018) at their native resolution (0.1° latitude x 0.1° longitude) in Figure 1b. EDGAR is used in the GMI CTM, but is overwritten by regional inventories, if available. Elevated O_3 concentrations generally coincide with industrialized regions that have high precursor emissions (Figure 1a). However, there are areas with high emissions and low O_3 or vice versa. For example, central Asia has low NO_x emissions (Figure 1b) but mean summertime O_3 in central Asia is generally > 50 ppbv, suggesting there is more at play than these anthropogenic emissions alone.

We evaluate whether the modeled O_3 distribution shown in Figure 1a is realistic using the correlation coefficient (r), calculated for CTM grid cells containing *in-situ* monitors (Section 2.2). The temporal correlation between modeled and observed $O_3 > 0.5$ in the vast majority of grid cells (Figure 2). The strength of the correlation is slightly weaker in central China than other parts of China or Europe and North America (compare Figure 2c with 2a-b), but there are no other readily-detectable spatial patterns regarding the strength of the correlation.

The primary goal of our study is to document the O_3-meteorology relationships in terms of the strength of the temporal correlation of O_3 with temperature and humidity. Thus, the model's ability to reproduce the temporal variability of O_3 (Figure 2) is the relevant litmus test for model performance. As the strength of the temporal correlation is consistent from region to region and in light of recent work showing that the GMI CTM has skill in capturing the O_3-temperature relationships (Strode et al., 2015; Kerr et al., 2019), we believe the GMI CTM is a suitable tool to meet our goal. The agreement between the observed and modeled O_3-meteorology correlations will be explored in the following section (Section 4), and this analysis will also support our use of the GMI CTM to simulate the covariance between O_3 and temperature or humidity.

4 O_3-meteorology relationships

In this section we describe the relationships among O_3, temperature, and humidity on daily timescales in the Northern Hemisphere during summer. We primarily use the GMI CTM but also compare the modeled relationships to observed values. As discussed in the Introduction (Section 1), other studies have focused mainly on subsets of the Northern Hemisphere mid-latitudes, while our examination of the relationships across the entire hemisphere allows us to have a more holistic sense of the synoptic-scale variations of these relationships.

In the mid-latitudes ($\sim 30-60°$N), statistically-significant positive values of $r(T, O_3)$ are simulated by the CTM throughout continental regions of North America and Eurasia (Figure 3a), but over all oceans $r(T, O_3)$ is negative. Poleward of the mid-latitudes, the strength of $r(T, O_3)$ decreases nearly monotonically over land, reaching either weak, insignificant values or significantly negative correlations (Figure 3a). The O_3-temperature relationship is varied equatorward of the mid-latitudes over land, but generally the strength of $r(T, O_3)$ decreases to insignificant values or significantly negative values (Figure 3a). Previous work by Rasmussen et al. (2012) and Brown-Steiner et al. (2015) in the U.S. and Han et al. (2020) and Lu, Zhang, Chen, et al. (2019) in China showed a similar latitudinal gradient of $r(T, O_3)$. Despite the general tendency of a positive-to-negative relationship between O_3 and temperature with decreasing latitude, there are regions at low latitudes with significant positive correlations between O_3 and temperature (Indo-Gangetic Plain, Sahel; Figure 3a).

Similar to $r(T, O_3)$, the strength of $r(q, O_3)$ transitions from significantly positive in the mid-latitudes to significantly negative at higher and lower latitudes, notwithstanding parts of the Middle East and southeast Asia (Figure 3b). These results are supported by modeling and observational studies in the U.S. and China, which indicate $r(q, O_3) > 0$ in the northern U.S. and China and $r(q, O_3) < 0$ in southern U.S. and China (e.g., Tawfik & Steiner, 2013; Kavassalis & Murphy, 2017; Li et al., 2019). Specific humidity and O_3 are also significantly anticorrelated over the oceans.

In continental regions of the mid-latitudes, the O_3-meteorology correlations suggest that temperature is a better predictor of O_3 than specific humidity, as $r(T, O_3) > r(q, O_3)$. Other studies support temperature as a leading covariate in the mid-latitudes (e.g., Camalier et al., 2007; Porter et al., 2015; Otero et al., 2016; Sun et al., 2017; Kerr & Waugh, 2018).

Many other studies report dO_3/dT (Rasmussen et al., 2012; S. Zhao et al., 2013; Brown-Steiner et al., 2015; Kerr et al., 2019; Porter & Heald, 2019), and we also present dO_3/dT and dO_3/dq in Figure SI1 for comparisons with these other studies. The spatial variations of the slopes shown in Figure SI1 are qualitatively similar to $r(T, O_3)$ and $r(q, O_3)$ shown in Figure 3, as is expected by construction.

To test whether the modeled O_3-meteorology relationships are realistic, we calculate $r(T, O_3)$ and $r(q, O_3)$ from the *in-situ* networks described in Section 2.2. The strength of the zonally-averaged values of observed and modeled $r(T, O_3)$ and $r(q, O_3)$ generally reaches a maximum around 50°N across four distinct regions (Figure 4). In Europe and the eastern U.S., the CTM slightly overestimates the strength of $r(T, O_3)$ and $r(q, O_3)$ by $\sim 0.1-0.3$, similar to other studies (e.g., Brown-Steiner et al., 2015; Kerr et al., 2019). Observations are sparse outside of the mid-latitudes. A small number of AQS monitors in Alaska and NAPS monitors in northern Canada support the transition of $r(T, O_3)$ and $r(q, O_3)$ from positive to negative at high latitudes that is suggested by the model (Figure 4).

In summary, the observation- and model-based analysis of the relationships among surface-level O_3 and temperature or humidity reveals substantial variability across the Northern Hemisphere during summer. Within a mid-latitude band ($\sim 30-60$°N) over land, O_3 is significantly correlated with temperature and humidity (Figures 3-4). Over the oceans and outside of the mid-latitudes, the strength of the O_3-relationships are either near-zero or significantly negative (Figures 3-4). These results suggest positive O_3-meteorology relationships are the exception, not the norm, over the entire hemispheric domain.

5 Factors causing the O_3-meteorology relationships

The O_3-meteorology relationships in Figure 3 are far from uniform, and their spatial structure begs the question: what factors drive these relationships? In Section 1, we discussed several direct and indirect drivers that have been linked to O_3 variability, such as emissions, chemistry, and transport. Recent work has shown that transport-related processes are key contributors to the O_3-temperature relationship in the U.S. and Europe (Kerr et al., 2019; Porter & Heald, 2019), and we expand on these previous findings and examine the covariance of O_3 with temperature and humidity over the Northern Hemisphere. We do this using the transport-only GMI CTM simulation in which the daily variability of chemistry and emissions are fixed (Section 2.1).

The difference in the magnitudes of $r(T, O_3)$ and $r(q, O_3)$ calculated between the control and transport-only simulations (Figure 5) demonstrates that considering only daily variations in transport-related processes yields O_3-meteorology relationships of similar magnitude as in the control simulation (Figure 3). Over all the oceans and a majority of the continental regions in the Northern Hemisphere, the strength of $r(T, O_3)$ and $r(q, O_3)$

increases or decreases < 0.1 (Figure 5). The hatching in Figure 5 demonstrates that the significance of the O_3-meteorology relationships is largely retained when only daily variations in transport-related processes are considered. This further supports the role of transport as the key driver of the O_3-meteorology relationships.

There are a few continental regions with significant O_3-meteorology correlations in the control simulation where r decreases or increases by up to ~ 0.5 and becomes insignificant (e.g., southern U.S. and southeast Asia for $r(T, O_3)$ and the southwestern U.S. for $r(q, O_3)$ in Figure 5). In these regions, the daily variability of chemistry and emissions appears important for the significance of the O_3-meteorology correlations, and further work is warranted to understand the roles of meteorology, chemistry, and emissions on O_3.

These results answer our original question whether transport, chemistry, or emissions are responsible for the O_3-meteorology relationships, but they also raise the question of which aspect(s) of transport links temperature and humidity to O_3. In the next section we explore the role of the jet stream on surface-level temperature, humidity, and O_3, and we also develop and test hypotheses to link synoptic-scale flow aloft to meteorology and composition at the surface.

5.1 The role of the jet stream

Barnes and Fiore (2013) determined that the largest O_3 variability and peak strength of $r(T, O_3)$ are located near ϕ_{jet} in the eastern U.S. These results were further explored by Shen et al. (2015) who found that O_3 responded to seasonal variations in the position of the jet stream and that a poleward shift of the jet increased O_3 concentrations south of the jet. In this section we expand upon this previous work and document the response of surface-level O_3, temperature, and humidity to daily changes in ϕ_{jet} across the Northern Hemisphere.

The time-averaged latitude of the jet stream ($\overline{\phi_{jet}}$) is shown by the scatter points in Figure 1, and $\overline{\phi_{jet}}$ averaged over the entire hemisphere is 50.1°N. The variability of the jet, cast in terms of the standard deviation ($\sigma_{\phi_{jet}}$), averaged over the Northern Hemisphere is 10.5°, but its variability is not constant throughout the hemisphere (error bars in Figure 1). Rather, we note the largest variability over continental regions, particularly Eurasia ($\sim 20°$), and smaller variability over maritime regions, coinciding with the Atlantic and Pacific storm tracks. ϕ_{jet} is only one metric to describe the jet stream, and other jet-related measures exist (e.g., strength of the jet, waviness). Our focus on ϕ_{jet} rather than other metrics is based on Ordóñez et al. (2019) who found that ϕ_{jet} exerts a stronger influence than the strength of the jet on surface-level pollution extremes.

The maximum variability of O_3 (Figure 1) and the strength of the O_3-meteorology correlations (Figures 3-5) peak at or slightly south of ϕ_{jet}, and ϕ_{jet} also separates regions with elevated O_3 concentrations to its south from regions with low (< 30 ppbv) concentrations to its north (Figure 1a). These results are consistent with Barnes and Fiore (2013); however, it is worth pointing out a couple of exceptions: (1) In Asia, O_3 variability peaks over a broader latitudinal range, extending from southward to $\sim 20°$N (Figure 1). (2) There are regions with significant positive values of $r(T, O_3)$ such as the Sahel and India that do not coincide with ϕ_{jet} (Figure 3a). These results expand upon Barnes and Fiore (2013), who only examined latitudes within $\sim 15°$ of the jet in eastern North America. Our current work also reveals the weak-to-negative correlation between O_3 and humidity or temperature for marine environments and subtropical and high latitude locations.

To further examine the role of the jet stream on the O_3-meteorology relationships, we segregate summer days into two subsets: days when the jet stream is in poleward (PW) and equatorward (EW) positions. Days classified as PW (EW) are days in which ϕ_{jet}

exceeds (is less than) the 70th (30th) percentile of all daily ϕ_{jet} at each longitudinal grid cell. We construct composites of O_3, temperature, and humidity by identifying the average value of these fields on days with a PW or EW jet stream and thereafter calculate the difference of these PW and EW composites.

The difference in the PW and EW composites (PW - EW) of O_3, temperature, and humidity are positive in the mid-latitudes over land (Figure 6), which indicates that these fields increase when the jet is in a more northerly position. The positive values are generally significant (hatching in Figure 6), coincide with the latitudinal band over which the jet stream migrates, and persist $10-15°$ north and south of its mean position over land. Outside the continental mid-latitudes, the association between the position of the jet and O_3, temperature, or humidity is weak and insignificant (Figure 6).

In contrast, there is a difference in the response of O_3 to the jet stream versus temperature and humidity over the mid-latitude ocean basins. In the case of O_3, a poleward movement of the jet decreases O_3 (Figure 6a), which could reflect asymmetries in the source regions of O_3 precursors between the land and ocean. On the other hand, temperature and humidity increase as the jet shifts poleward, akin to the behavior of these variables over land (Figure 6b-c). The impact of the jet stream on O_3, temperature, and humidity outside of the mid-latitudes is largely insignificant (Figure 6).

For completeness, maps of the correlation of jet distance with the variables in Figure 6 are shown in Figure SI2. We note that the strength of the correlation between ϕ_{jet} and O_3 and meteorology is weaker than $r(T, O_3)$ and $r(q, O_3)$, and the spatial extent of areas with significant correlations is smaller (compare Figures 3 and SI2).

While the response of O_3 and meteorological fields to the meridional movement of the jet stream is consistent in its sign in the mid-latitudes over land, there are some regions outside of the continental mid-latitudes where jet movement leads to increases of one variable and decreases of another. China is an example of this. As the jet migrates poleward, O_3 significantly increases, as it does throughout the mid-latitudes; however, temperature remains more or less constant, and humidity slightly decreases (Figures 6, SI2). This discrepancy and others evident in Figures 6 and SI2, particularly those at lower latitudes and over the oceans, are beyond the scope of this study, but future studies should further examine and address regions where O_3, temperature, and humidity are decoupled from the jet in this manner.

Having uncovered the dominant role of transport and the connections with the jet, we next explore transport-related processes that might be responsible for the relationships among surface-level O_3, the jet stream, and meteorology. As cyclones are commonly-invoked to explain O_3 variability, we begin by showing the impact of the jet stream on cyclone frequency and, in turn, the effect of cyclones on O_3. We then show and discuss the how the jet stream affects the mean meridional circulation and commensurate fluxes of O_3, heat, and moisture.

5.2 Cyclones

Mid-latitude baroclinic cyclones follow a storm track dictated by the jet stream, and changes in ϕ_{jet} affect the location of this storm track (e.g., Shen et al., 2015). To assess the dependence of cyclone frequency on ϕ_{jet}, we show the spatial distribution of the climatological frequency of cyclones detected by MCMS (Section 2.4.3) in Figure 7a. The highest frequency of mid-latitude cyclone detections largely follows ϕ_{jet} and is offset north of the jet by $\sim 10°$ over North America. In other regions such as eastern Asia, the peak cyclone frequency occurs in a broader latitudinal band, extending north and south of ϕ_{jet} by $\sim 15°$ (Figure 7a).

We identify the subset of days with a poleward-shifted or equatorward-shifted jet using the 70th and 30th percentiles of the daily latitudes of the jet stream, as previously described, to determine the dependence of cyclones on ϕ_{jet}. We thereafter determined the frequency of cyclones on these subsets of days and found the difference (Figure 7b). The meridional movement of the jet affects cyclones in two different ways. First, the total number of cyclones on days when the jet is in a poleward position is 15% less than on days when the jet is equatorward. Second, the preferred location of cyclones ("storm track") shifts alongside the jet, and cyclones are more highly concentrated about ϕ_{jet} when the jet is equatorward compared to when it is poleward (Figure 7b).

The decrease and latitudinal shift in cyclone frequency with meridional movements of the jet stream could be the transport-related mechanism responsible for the above O_3-meteorology relationships. The cold fronts associated with mid-latitude cyclones have been suggested as a mechanism for the ventilation of the eastern U.S. (Mickley, 2004), and Knowland et al. (2015) and Jaeglé et al. (2017) demonstrated how cyclones redistribute O_3, its precursors, and other pollutants vertically and horizontally in the atmosphere. We assess the impact of cyclones on surface-level O_3 by further filtering the cyclones from the MCMS dataset (Section 2.4.3), requiring that a particular cyclone (1) occurs over land and (2) is detected for ≥ 2 six-hourly time steps to allow us to calculate the direction of propagation. We then rotate cyclones following Knowland et al. (2015) and Knowland et al. (2017) such that they propagate to the right of Figure 8 to account for the impact of different ascending and descending airstreams within the cyclones. Applying these filters to cyclones in summers $2008-2010$ yields ~ 730 cyclones with an average lifetime of ~ 54 hours. The mean direction of cyclone propagation is east-southeast ($\sim 120°$, where $0°$ is north). Though we have only considered cyclones occurring over land in this analysis, compositing all land- and ocean-based cyclones produces O_3 anomalies of similar magnitude.

We observe that the largest negative O_3 anomaly occurs in the "cold sector" of the cyclone, whereas a positive anomaly occurs in the "warm sector," but these positive and negative anomalies cancel each other when averaged over the footprint of the cyclones leading to a net ~ 0 ppbv change in O_3 (Figure 8). Comparing our results with conceptual models of baroclinic cyclones (e.g., Polvani & Esler, 2007) hints that the positive anomalies occur near the warm conveyor belt, while negative anomalies occur near the dry intrusion where there is likely an influence of air from the free troposphere or lower stratosphere.

If cyclones were the mechanism that linked ϕ_{jet} to surface-level O_3, we might expect that the cyclones-driven impact on O_3 would be > 6 ppbv in the mid-latitudes, similar to the impact that ϕ_{jet} has on O_3 (Figure 6a). However, our analysis in Figure 8 indicates that, on average, cyclones have a much weaker effect on surface-level O_3, despite the connections between cyclones and the jet stream (Figure 7b). We do note that there is substantial variability among individual cyclones (the standard deviation of the O_3 anomaly is a factor of ~ 6 greater than the largest anomaly; Figure 8), so some cyclones might be effective at reducing surface-level O_3, but this is far from the case for all cyclones.

Other studies support the small role of cyclones on surface-level O_3. Knowland et al. (2015) showed that the surface-level O_3 anomaly associated with springtime cyclones in the North Atlantic and Pacific is small (i.e., $-5 < \delta\, O_3 < 5$ ppbv); however, they found a larger impact when examining the mid- to upper-level O_3 anomalies. Moreover, Leibensperger et al. (2008) found a negative correlation between the number of O_3 pollution events and the number of mid-latitude cyclones passing through the southern climatological storm track ($\sim 40-50°$N) over eastern North America on interannual timescales, but Turner et al. (2012) demonstrated that this correlation is weak, and cyclone frequency explains less than 10% of the variability of O_3 pollution events in the region.

In summary, while the storm track dictating the preferred location of baroclinic cyclones shifts with the jet (Figure 7b), cyclones are likely not the key mechanism controlling O_3 variability in the Northern Hemisphere mid-latitudes as they only explain a small fraction of the changes of O_3 associated with daily migrations of the jet (Figure 8).

5.3 Zonal mean meridional transport

An analysis of PBLH, near-surface zonal flow, and near-surface total wind are either not significantly influenced by ϕ_{jet} or cannot explain the magnitude of jet-related changes in O_3 (Text SI1-SI2 and Figures SI3-4). In contrast, the increase in the near-surface meridional flow (V_{10}) as the jet shifts poleward (Text SI2, Figures SI3c, SI4c) accompanied by increases in O_3, temperature, and humidity (Figures 6, SI2) suggest that changes in the mean meridional flow may play a major role in the relationships among the jet stream, O_3, and meteorology. To examine this further, we next calculate the meridional fluxes of O_3, heat, and moisture; the contributions from the zonal mean and eddy components; and how the jet influences these fluxes.

To distinguish contributions from the eddy and the mean components of the total flux, we decompose the total flux of a given field X into deviations from its time and zonal means. The time mean is denoted by $\overline{X}$, and deviations from the time mean are denoted X', such that $X = \overline{X}+X'$. We denote the zonal mean by $[X]$, and deviations from the zonal mean are given by X^*, so that $X = [X] + X^*$ (e.g., Peixoto & Oort, 1992; Kaspi & Schneider, 2013). The time-averaged zonal mean O_3 flux by the near-surface meridional wind can be expressed by

$$[\overline{V_{10}\, O_3}] = [\overline{V_{10}}][\overline{O_3}] + [\overline{V_{10}^*}\, \overline{O_3^*}] + [\overline{V_{10}'\, O_3'}], \qquad (1)$$

where the terms on the righthand side of Equation 1 represent the contributions from the mean meridional circulation, stationary eddies, and transient eddies, respectively. Similar expressions can be derived for temperature and humidity. Note that in our analysis, we sum the contributions from the stationary and transient eddies and refer to them as the "eddy" contribution.

In the zonal mean, the contribution from eddies and the mean meridional circulation for O_3 and temperature on all days are qualitatively similar (Figure 9a, d). For these fields, eddies play a small role, regardless of latitude, while the mean meridional circulation leads to a equatorward (poleward) O_3 and heat flux for $\phi < 40°$N ($\phi > 40°$N). Eddies play a larger role in shaping the total flux of humidity for $\phi < 45°$N than for temperature or O_3 (compare Figure 9g with Figure 9a, d), but the eddies make a negligible contribution to the total moisture flux at higher latitudes (Figure 9g). While heat transport in the Northern Hemisphere mid-latitudes is often attributed to eddies, this only holds for boreal winter or annual means, not boreal summer (Hartmann, 2007).

If we recalculate the fluxes for the subsets of days when the jet is PW and EW, a striking feature is revealed: there is a large difference in the sign and magnitude of O_3, temperature, and humidity flux by the mean meridional circulation (Figure 9b-c, e-f, h-i). The relatively small total flux of these fields in the mid-latitudes on all days (Figure 9a, d, g) can be viewed as the cancellation of a large positive (poleward) flux on days when the jet is PW (Figure 9b, e, h) and large negative (equatorward) flux on days when the jet is EW (Figure 9c, f, i). There is a consistent contribution from the eddy component whether all days or days when the jet is PW or EW are considered. Although we only have shown the flux of O_3, temperature, and humidity using surface-level fields here, using fields averaged over the lower troposphere (1000−800 hPa) does not change our conclusions.

In the mid-latitudes over land, V_{10} and the flux of O_3, temperature, and humidity by the mean meridional circulation responds to changes in the position of the jet stream such that when the jet is PW, increased northerly flow transports O_3, heat, and moisture northward (Figures SI3c, SI4c, 9). This yields positive relationships among O_3, meteorology, and the jet stream.

Over the mid-latitude oceans, O_3 does not have the monotonically decreasing latitudinal gradient as it does over land (Figure 1a); rather, O_3 increases slightly increases with latitude in the vicinity of the North Atlantic and North Pacific storm tracks ($\sim 50-60°$N), potentially reflecting transient baroclinic cyclones ventilating continental regions and sweeping O_3 (and its precursors) to sea. Increased poleward meridional flow when the jet migrates north over the oceans (Figure SI3c, SI4c) could advect *lower* concentrations of O_3 poleward (Figure 6a), while advecting *higher* temperature and humidity poleward (Figure 6b-c). This mismatch in sign between O_3 and temperature or humidity could contribute to the negative O_3-meteorology-jet relationships over the oceans. While this can explain some of the negative correlation of O_3 with temperature and humidity over the oceans in the mid-latitudes, it cannot explain the widespread negative O_3-meteorology relationships over all ocean basins.

Outside of the mid-latitudes, ϕ_{jet} is not linked to changes in the eddy versus zonal mean contributions to the total flux of O_3, heat, and moisture. Accordingly, the relationships among O_3, the jet stream, and temperature or humidity have mixed strength and sign outside the mid-latitudes (Figures 3, 6, 9).

It is important to note that the eddy contribution to the total flux (Equation 1, Figure 9) encompasses more than just transient baroclinic cyclones. Implicit in this term are contributions from stationary centers of action such as the Bermuda High and Pacific High. Additionally, processes occurring within these systems such as stratospheric-tropospheric exchanges are included within our calculation of the eddy fluxes.

We have also conducted a similar decomposition of the fluxes of O_3 precursors such as NO_x and CO (not shown) and found that these species respond similarly to changes in ϕ_{jet}. Thus, we cannot explicitly rule out whether the O_3-meteorology-jet relationships are solely the result of the transport of O_3 versus the transport of its precursor species leading to subsequent chemical production.

The connection between the mean meridional circulation and O_3 variability has been the subject of a recent study by Lu, Zhang, Zhao, et al. (2019). This study related increasing trends in Southern Hemisphere tropospheric O_3 with changes in the mean meridional circulation (i.e., the Southern Hemisphere Hadley Cell). Specifically, it was suggested that changes in extratropical stratospheric-to-tropospheric transport, associated with the Hadley Cell, can foster the transport of O_3-rich air to the troposphere and redistribute O_3 precursors (Lu, Zhang, Zhao, et al., 2019).

6 Conclusions

The primary intent of this study was to document the relationships among surface-level O_3, temperature, and humidity and explore the cause(s) of these relationships. Both observations and the GMI CTM support substantial spatial variations in $r(T, O_3)$ and $r(q, O_3)$. In continental regions of the mid-latitudes ($\sim 35-60°$N), the O_3-meteorology relationships are significantly positive (Figures 3-4), but outside of the mid-latitudes and over the oceans, $r(T, O_3)$ and $r(q, O_3)$ are either insignificant or significantly anticorrelated (Figure 3).

Our transport-only GMI CTM simulation indicates that the O_3-temperature and O_3-humidity relationships are largely the product an indirect association with transport across the Northern Hemisphere (Figure 5). This is consistent with previous work by Kerr et al. (2019) and Porter and Heald (2019), which showed that a majority of the O_3-temperature relationship in the U.S. and Europe derived from meteorological phenomena.

The variability of surface-level O_3, temperature, and humidity are linked to the meridional movement of the jet stream in the Northern Hemisphere mid-latitudes. This result extends previous work focusing on the eastern U.S. (e.g., Barnes & Fiore, 2013; Shen et al., 2015) to the entire Northern Hemisphere. Over land in the mid-latitudes, a poleward (equatorward) shift of the jet is associated with increased (decreased) surface-level O_3, temperature, and humidity (Figures 6, SI2). Over the oceans, temperature and humidity respond to this meridional movement of the jet in the same fashion as over land, but the poleward (equatorward) movement of the jet decreases (increases) O_3. Changes in cyclone frequency, $PBLH$, and strength of the near-surface winds are either not connected with movements of the jet or do not result in substantial changes in surface O_3 (Figures 7-8, SI3-SI4).

We ultimately found that the jet influences these surface-level fields by means of changes in the mean meridional circulation. On days when the jet is in a poleward (equatorward) position, the mean meridional circulation is responsible for a large poleward (equatorward) flux of heat, moisture, and O_3 in the mid-latitudes (Figure 9). While this holds in the zonal mean, we have shown clear land-ocean differences in the relationships among O_3, temperature or specific humidity, and the jet stream (Figures 3, 6, SI2). These differences could stem from differences in meridional gradients of O_3 and its precursors between the continental and marine regions of the Northern Hemisphere (e.g., Figure 1b). Our future work will elucidate how the source region of emissions impacts the relationship between the jet stream and surface-level composition and investigate why the land-ocean differences exist.

Establishing the spatial variations of the O_3-meteorology relationships is a prerequisite to understand which regions could experience an "O_3-climate penalty" (Wu et al., 2008) under future climatic changes. As the O_3-meteorology relationships in the present-day climate are far from uniform in both magnitude and sign, it is unlikely that future changes in the climate will affect O_3 uniformly. Furthermore, as the relationships among O_3, temperature, and humidity are driven by an indirect association with transport, caution should be used when applying any measures of the current sensitivity of O_3 to meteorological variables (e.g., dO_3/dT or dO_3/dq from Figure SI1) to future climatic changes.

Overall, our results demonstrate the importance of the position of the jet stream and mean meridional circulation on O_3 variability in the Northern Hemisphere, both of which will be affected by the future climate (e.g., Barnes & Polvani, 2013; Shaw & Voigt, 2015; Grise et al., 2019). A robust poleward displacement of the jet stream is expected in the twenty-first century, while changes to other properties of the jet (i.e., variations in speed; north-south movement) will exhibit spatial heterogeneity (Barnes & Polvani, 2013). The effect of these changes on surface-level O_3 needs to be explored.

Acknowledgments

G. H. Kerr is supported by the NSF IGERT Program (Grant No. 1069213). The MERRA-2 data used in this study have been provided by the Global Modeling and Assimilation Office (GMAO) at NASA Goddard Space Flight Center. The data may be obtained at `gmao.gsfc.nasa.gov/reanalysis/MERRA-2/`. NASA GMI CTM output is publicly available on the data portal for the NASA Center for Climate Simulation (`portal.nccs.nasa.gov/datashare/dirac`). The control simulation can be found at the following path: `/gmidata2/users/mrdamon/Hindcast-Family/HindcastMR2/`. Hourly observations of O_3 are available for (1) China at `beijingair.sinaapp.com`, (2) the European Union at `projects.nilu.no//ccc/emepdata.html`, (3) Canada at `maps-cartes.ec.gc.ca/rnspa-naps/data.aspx`, and (4) the U.S. at `aqs.epa.gov/aqsweb/airdata/`

`download_files.html`. MCMS development is supported by NASA's Earth Science Program for Modeling, Analysis, and Prediction (MAP), and data can be found at `gcss-dime.giss.nasa.gov/mcms/`.

References

Barnes, E. A., & Fiore, A. M. (2013). Surface ozone variability and the jet position: Implications for projecting future air quality. *Geophys. Res. Lett.*, *40*(11), 2839–2844. doi: 10.1002/grl.50411

Barnes, E. A., & Polvani, L. (2013). Response of the midlatitude jets, and of their variability, to increased greenhouse gases in the CMIP5 models. *J. Clim.*, *26*(18), 7117–7135. doi: 10.1175/JCLI-D-12-00536.1

Barrett, B. S., Raga, G. B., Retama, A., & Leonard, C. (2019). A multiscale analysis of the tropospheric and stratospheric mechanisms leading to the March 2016 extreme surface ozone event in Mexico City. *J. Geophys. Res.*, *124*(8), 4782–4799. doi: 10.1029/2018JD029918

Bauer, M., & Genio, A. D. D. (2006). Composite analysis of winter cyclones in a GCM: Influence on climatological humidity. *J. Clim.*, *19*(9), 1652–1672. doi: 10.1175/jcli3690.1

Bauer, M., Tselioudis, G., & Rossow, W. B. (2016). A new climatology for investigating storm influences in and on the extratropics. *J. Appl. Meteorol. Climatol.*, *55*(5), 1287–1303. doi: 10.1175/jamc-d-15-0245.1

Bosilovich, M., Akella, S., Coy, L., Cullather, R., Draper, C., Gelaro, R., et al. (2015). *MERRA-2: Initial evaluation of the climate, NASA/TM–2015-104606* (Vol. 43).

Brown-Steiner, B., Hess, P., & Lin, M. (2015). On the capabilities and limitations of GCCM simulations of summertime regional air quality: A diagnostic analysis of ozone and temperature simulations in the US using CESM CAM-Chem. *Atmos. Environ.*, *101*, 134–148. doi: 10.1016/j.atmosenv.2014.11.001

Camalier, L., Cox, W., & Dolwick, P. (2007). The effects of meteorology on ozone in urban areas and their use in assessing ozone trends. *Atmos. Environ.*, *41*(33), 7127–7137. doi: 10.1016/j.atmosenv.2007.04.061

Cooper, O. R., Gao, R.-S., Tarasick, D., Leblanc, T., & Sweeney, C. (2012). Long-term ozone trends at rural ozone monitoring sites across the United States, 1990–2010. *J. Geophys. Res.*, *117*, D22307. doi: 10.1029/2012JD018261

Crippa, M., Guizzardi, D., Muntean, M., Schaaf, E., Dentener, F., van Aardenne, J. A., et al. (2018). Gridded emissions of air pollutants for the period 1970–2012 within EDGAR v4.3.2. *Earth Syst. Sci. Data*, *10*(4), 1987–2013. doi: 10.5194/essd-10-1987-2018

Dawson, J. P., Adams, P. J., & Pandis, S. N. (2007). Sensitivity of ozone to summertime climate in the eastern USA: A modeling case study. *Atmos. Environ.*, *41*(7), 1494–1511. doi: 10.1016/j.atmosenv.2006.10.033

Dee, D. P., Uppala, S. M., Simmons, A. J., Berrisford, P., Poli, P., Kobayashi, S., et al. (2011). The ERA-Interim reanalysis: Configuration and performance of the data assimilation system. *Q. J. R. Meteorol. Soc.*, *137*(656), 553–597. doi: 10.1002/qj.828

Derwent, R. G., Witham, C. S., Utembe, S. R., Jenkin, M. E., & Passant, N. R. (2010). Ozone in central England: The impact of 20 years of precursor emission controls in Europe. *Environ. Sci. Policy*, *13*(3), 195–204. doi: 10.1016/j.envsci.2010.02.001

Duncan, B. N., Strahan, S. E., Yoshida, Y., Steenrod, S. D., & Livesey, N. (2007). Model study of the cross-tropopause transport of biomass burning pollution. *Atmos. Chem. Phys.*, *7*(14), 3713–3736.

Duncan, B. N., West, J. J., Yoshida, Y., Fiore, A. M., & Ziemke, J. R. (2008). The influence of European pollution on ozone in the Near East and northern

Africa. *Atmos. Chem. Phys.*, *8*(8), 2267–2283. doi: 10.5194/acp-8-2267-2008

ECCC. (2017). *National air pollution surveillance program.* https://open.canada.ca/data/en/dataset/1b36a356-defd-4813-acea-47bc3abd859b. (Retrieved on 22 July 2019)

EPA. (2019). *Air quality system data mart.* http://www.epa.gov/ttn/airs/aqsdatamart. (Retrieved on 23 July 2019)

Fiore, A. M., Naik, V., & Leibensperger, E. M. (2015). Air quality and climate connections. *J. Air Waste Manage.*, *65*(6), 645–685. doi: 10.1080/10962247.2015.1040526

Gelaro, R., McCarty, W., Suárez, M. J., Todling, R., Molod, A., Takacs, L., et al. (2017). The Modern-Era Retrospective Analysis for Research and Applications, Version 2 (MERRA-2). *J. Clim.*, *30*(14), 5419–5454. doi: 10.1175/JCLI-D-16-0758.1

Grise, K. M., Davis, S. M., Simpson, I. R., Waugh, D. W., Fu, Q., Allen, R. J., et al. (2019). Recent tropical expansion: Natural variability or forced response? *J. Clim.*, *32*(5), 1551–1571. doi: 10.1175/jcli-d-18-0444.1

Guo, J. J., Fiore, A. M., Murray, L. T., Jaffe, D. A., Schnell, J. L., Moore, C. T., & Milly, G. P. (2018). Average versus high surface ozone levels over the continental USA: Model bias, background influences, and interannual variability. *Atmos. Chem. Phys.*, *18*(16), 12123–12140. doi: 10.5194/acp-18-12123-2018

Han, H., Liu, J., Shu, L., Wang, T., & Yuan, H. (2020). Local and synoptic meteorological influences on daily variability of summertime surface ozone in eastern China. *Atmos. Chem. Phys.*, 203–222. doi: 10.5194/acp-20-203-2020

Hartmann, D. L. (2007). The atmospheric general circulation and its variability. *J. Meteorol. Soc. Jpn. Ser. II*, *85B*(0), 123–143. doi: 10.2151/jmsj.85b.123

He, H., Stehr, J. W., Hains, J. C., Krask, D. J., Doddridge, B. G., Vinnikov, K. Y., et al. (2013). Trends in emissions and concentrations of air pollutants in the lower troposphere in the Baltimore/Washington airshed from 1997 to 2011. *Atmos. Chem. Phys.*, *13*(15), 7859–7874. doi: 10.5194/acp-13-7859-2013

Hegarty, J., Mao, H., & Talbot, R. (2007). Synoptic controls on summertime surface ozone in the northeastern United States. *J. Geophys. Res.*, *112*(D14). doi: 10.1029/2006JD008170

Hjellbrekke, A.-G., & Solberg, S. (2019). *Ozone measurements 2017* (EMEP/CCC-Report No. 2/2019). Kjeller, Norway: EMEP Co-operative Programme for Monitoring and Evaluation of the Long-range Transmission of Air Pollutants in Europe. Retrieved from https://projects.nilu.no//ccc/reports/cccr2-2019_Ozone.pdf

Jacob, D. J., & Winner, D. A. (2009). Effect of climate change on air quality. *Atmos. Environ.*, *43*(1), 51–63. doi: 10.1016/j.atmosenv.2008.09.051

Jaeglé, L., Wood, R., & Wargan, K. (2017). Multiyear composite view of ozone enhancements and stratosphere-to-troposphere transport in dry intrusions of Northern Hemisphere extratropical cyclones. *J. Geophys. Res.*, *122*(24), 13,436–13,457. doi: 10.1002/2017jd027656

Kaspi, Y., & Schneider, T. (2013). The role of stationary eddies in shaping midlatitude storm tracks. *J. Atmos. Sci.*, *70*(8), 2596–2613. doi: 10.1175/jas-d-12-082.1

Kavassalis, S. C., & Murphy, J. G. (2017). Understanding ozone-meteorology correlations: A role for dry deposition. *Geophys. Res. Lett.*, *44*(6), 2922–2931. doi: 10.1002/2016GL071791

Kerr, G. H., & Waugh, D. W. (2018). Connections between summer air pollution and stagnation. *Environ. Res. Lett.*, *13*(8), 084001. doi: 10.1088/1748-9326/aad2e2

Kerr, G. H., Waugh, D. W., Strode, S. A., Steenrod, S. D., Oman, L. D., & Strahan, S. E. (2019). Disentangling the drivers of the summertime ozone-temperature relationship over the United States. *J. Geophys. Res.*, *124*(19), 10503–10524.

doi: 10.1029/2019jd030572

Kim, S.-W., Heckel, A., McKeen, S. A., Frost, G. J., Hsie, E.-Y., Trainer, M. K., et al. (2006). Satellite-observed U.S. power plant NO_x emission reductions and their impact on air quality. *Geophys. Res. Lett.*, *33*(22). doi: 10.1029/2006GL027749

Knowland, K. E., Doherty, R. M., & Hodges, K. I. (2015). The effects of springtime mid-latitude storms on trace gas composition determined from the MACC reanalysis. *Atmos. Chem. Phys.*, *15*(6), 3605–3628. doi: 10.5194/acp-15-3605-2015

Knowland, K. E., Doherty, R. M., Hodges, K. I., & Ott, L. E. (2017). The influence of mid-latitude cyclones on European background surface ozone. *Atmos. Chem. Phys.*, *17*(20), 12421–12447. doi: 10.5194/acp-17-12421-2017

Landrigan, P. J., Fuller, R., Acosta, N. J. R., Adeyi, O., Arnold, R., Basu, N., et al. (2018). The lancet commission on pollution and health. *Lancet*, *391*(10119), 462–512. doi: 10.1016/s0140-6736(17)32345-0

Lefohn, A. S., Malley, C. S., Smith, L., Wells, B., Hazucha, M., Simon, H., et al. (2018). Tropospheric ozone assessment report: Global ozone metrics for climate change, human health, and crop/ecosystem research. *Elem. Sci. Anth.*, *6*(1), 28. doi: 10.1525/elementa.279

Leibensperger, E. M., Mickley, L. J., & Jacob, D. J. (2008). Sensitivity of US air quality to mid-latitude cyclone frequency and implications of 1980–2006 climate change. *Atmos. Chem. Phys.*, *8*(23), 7075–7086.

Li, K., Jacob, D. J., Liao, H., Shen, L., Zhang, Q., & Bates, K. H. (2019). Anthropogenic drivers of 2013–2017 trends in summer surface ozone in China. *Proc. Natl. Acad. Sci. U.S.A.*, *116*(2), 422–427. doi: 10.1073/pnas.1812168116

Lin, M., Horowitz, L. W., Payton, R., Fiore, A. M., & Tonnesen, G. (2017). US surface ozone trends and extremes from 1980 to 2014: Quantifying the roles of rising Asian emissions, domestic controls, wildfires, and climate. *Atmos. Chem. Phys.*, *17*(4), 2943–2970. doi: 10.5194/acp-17-2943-2017

Lu, X., Zhang, L., Chen, Y., Zhou, M., Zheng, B., Li, K., … Zhang, Q. (2019). Exploring 2016–2017 surface ozone pollution over China: Source contributions and meteorological influences. *Atmos. Chem. Phys.*, *19*(12), 8339–8361. doi: 10.5194/acp-19-8339-2019

Lu, X., Zhang, L., Zhao, Y., Jacob, D. J., Hu, Y., Hu, L., et al. (2019). Surface and tropospheric ozone trends in the Southern Hemisphere since 1990: Possible linkages to poleward expansion of the Hadley circulation. *Sci. Bull.*, *64*(6), 400–409. doi: 10.1016/j.scib.2018.12.021

Meehl, G. A., Tebaldi, C., Tilmes, S., Lamarque, J.-F., Bates, S., Pendergrass, A., & Lombardozzi, D. (2018). Future heat waves and surface ozone. *Environ. Res. Lett.*, *13*(6), 064004. doi: 10.1088/1748-9326/aabcdc

Mickley, L. J. (2004). Effects of future climate change on regional air pollution episodes in the United States. *Geophys. Res. Lett.*, *31*(24). doi: 10.1029/2004GL021216

Mudelsee, M. (2003). Estimating Pearson's correlation coefficient with bootstrap confidence interval from serially dependent time series. *Math. Geol.*, *35*(6), 651–665. doi: 10.1023/b:matg.0000002982.52104.02

Mudelsee, M. (2014). *Climate time series analysis: Classical statistical and bootstrap methods* (2nd ed.). Cham, Heidelberg, New York, Dordrecht, London: Springer International Publishing. doi: 10.1007/978-3-319-04450-7

Ordóñez, C., Barriopedro, D., & García-Herrera, R. (2019). Role of the position of the North Atlantic jet in the variability and odds of extreme PM_{10} in Europe. *Atmos. Environ.*, *210*, 35–46. doi: 10.1016/j.atmosenv.2019.04.045

Otero, N., Sillmann, J., Schnell, J. L., Rust, H. W., & Butler, T. (2016). Synoptic and meteorological drivers of extreme ozone concentrations over Europe. *Environ. Res. Lett.*, *11*(2), 024005. doi: 10.1088/1748-9326/11/2/024005

Parrish, D. D., Law, K. S., Staehelin, J., Derwent, R., Cooper, O. R., Tanimoto, H., et al. (2012). Long-term changes in lower tropospheric baseline ozone concentrations at northern mid-latitudes. *Atmos. Chem. Phys.*, *12*(23), 11485–11504. doi: 10.5194/acp-12-11485-2012

Peixoto, J. P., & Oort, A. H. (1992). *Physics of climate* (2nd ed.). New York: Am. Inst. Phys.

Phalitnonkiat, P., Hess, P. G. M., Grigoriu, M. D., Samorodnitsky, G., Sun, W., Beaudry, E., et al. (2018). Extremal dependence between temperature and ozone over the continental US. *Atmos. Chem. Phys.*, *18*(16), 11927–11948. doi: 10.5194/acp-18-11927-2018

Polvani, L. M., & Esler, J. G. (2007). Transport and mixing of chemical air masses in idealized baroclinic life cycles. *J. Geophys. Res.*, *112*(D23), D23102. doi: 10.1029/2007JD008555

Porter, W. C., & Heald, C. L. (2019). The mechanisms and meteorological drivers of the ozone-temperature relationship. *Atmos. Chem. Phys.*, 13367–13381. doi: 10.5194/acp-2019-140

Porter, W. C., Heald, C. L., Cooley, D., & Russell, B. (2015). Investigating the observed sensitivities of air-quality extremes to meteorological drivers via quantile regression. *Atmos. Chem. Phys.*, *15*(18), 10349–10366.

Pusede, S. E., Steiner, A. L., & Cohen, R. C. (2015). Temperature and recent trends in the chemistry of continental surface ozone. *Chem. Rev.*, *115*(10), 3898–3918. doi: 10.1021/cr5006815

Rasmussen, D. J., Fiore, A., Naik, V., Horowitz, L., McGinnis, S., & Schultz, M. (2012). Surface ozone-temperature relationships in the eastern US: A monthly climatology for evaluating chemistry-climate models. *Atmos. Environ.*, *47*, 142–153. doi: 10.1016/j.atmosenv.2011.11.021

Rasmussen, D. J., Hu, J., Mahmud, A., & Kleeman, M. J. (2013). The ozone–climate penalty: Past, present, and future. *Environ. Sci. Technol.*, *47*(24), 14258–14266. doi: 10.1021/es403446m

Reddy, P. J., & Pfister, G. G. (2016). Meteorological factors contributing to the interannual variability of midsummer surface ozone in Colorado, Utah, and other western U.S. states. *J. Geophys. Res.*, *121*(5), 2434–2456. doi: 10.1002/2015JD023840

Sadiq, M., Tai, A. P. K., Lombardozzi, D., & Martin, M. V. (2017). Effects of ozone–vegetation coupling on surface ozone air quality via biogeochemical and meteorological feedbacks. *Atmos. Chem. Phys.*, *17*(4), 3055–3066. doi: 10.5194/acp-17-3055-2017

Schnell, J. L., Holmes, C. D., Jangam, A., & Prather, M. J. (2014). Skill in forecasting extreme ozone pollution episodes with a global atmospheric chemistry model. *Atmos. Chem. Phys.*, *14*(15), 7721–7739. doi: 10.5194/acp-14-7721-2014

Shaw, T. A., & Voigt, A. (2015). Tug of war on summertime circulation between radiative forcing and sea surface warming. *Nature Geosci.*, *8*(7), 560–566. doi: 10.1038/ngeo2449

Shen, L., Mickley, L. J., & Tai, A. P. K. (2015). Influence of synoptic patterns on surface ozone variability over the eastern United States from 1980 to 2012. *Atmos. Chem. Phys.*, *15*(19), 10925–10938. doi: 10.5194/acp-15-10925-2015

Simon, H., Reff, A., Wells, B., Xing, J., & Frank, N. (2015). Ozone trends across the United States over a period of decreasing NOx and VOC emissions. *Environ. Sci. Technol.*, *49*(1), 186–195. doi: 10.1021/es504514z

Strahan, S. E., Douglass, A. R., & Newman, P. A. (2013). The contributions of chemistry and transport to low arctic ozone in March 2011 derived from aura MLS observations. *J. Geophys. Res.*, *118*(3), 1563–1576. doi: 10.1002/jgrd.50181

Strahan, S. E., Duncan, B. N., & Hoor, P. (2007). Observationally derived transport diagnostics for the lowermost stratosphere and their application to the GMI chemistry and transport model. *Atmos. Chem. Phys.*, *7*(9), 2435–2445.

Strode, S. A., Rodriguez, J. M., Logan, J. A., Cooper, O. R., Witte, J. C., Lamsal, L. N., et al. (2015). Trends and variability in surface ozone over the United States. *J. Geophys. Res.*, *120*(17), 9020–9042. doi: 10.1002/2014JD022784

Sun, W., Hess, P., & Liu, C. (2017). The impact of meteorological persistence on the distribution and extremes of ozone. *Geophys. Res. Lett.*, *44*, 1545–1553. doi: 10.1002/2016GL071731

Tai, A. P., & Martin, M. V. (2017). Impacts of ozone air pollution and temperature extremes on crop yields: Spatial variability, adaptation and implications for future food security. *Atmos. Environ.*, *169*, 11–21. doi: 10.1016/j.atmosenv.2017.09.002

Tai, A. P., Mickley, L. J., & Jacob, D. J. (2010). Correlations between fine particulate matter ($PM_{2.5}$) and meteorological variables in the United States: Implications for the sensitivity of $PM_{2.5}$ to climate change. *Atmos. Environ.*, *44*(32), 3976–3984. doi: 10.1016/j.atmosenv.2010.06.060

Tarasick, D., Galbally, I. E., Cooper, O. R., Schultz, M. G., Ancellet, G., Leblanc, T., et al. (2019). Tropospheric ozone assessment report: Tropospheric ozone from 1877 to 2016, observed levels, trends and uncertainties. *Elem. Sci. Anth.*, *7*(1), 39. doi: 10.1525/elementa.376

Tawfik, A. B., & Steiner, A. L. (2013). A proposed physical mechanism for ozone-meteorology correlations using land–atmosphere coupling regimes. *Atmos. Environ.*, *72*, 50–59. doi: 10.1016/j.atmosenv.2013.03.002

Turner, A. J., Fiore, A. M., Horowitz, L. W., Naik, V., & Bauer, M. (2012). Summertime cyclones over the Great Lakes storm track from 1860–2100: Variability, trends, and association with ozone pollution. *Atmos. Chem. Phys.*, *12*(8), 21679–21712. doi: 10.5194/acpd-12-21679-2012

Varotsos, K. V., Tombrou, M., & Giannakopoulos, C. (2013). Statistical estimations of the number of future ozone exceedances due to climate change in Europe. *J. Geophys. Res.*, *118*(12), 6080–6099. doi: 10.1002/jgrd.50451

Wilks, D. S. (1997). Resampling hypothesis tests for autocorrelated fields. *J. Clim.*, *10*(1), 65–82. doi: 10.1175/1520-0442(1997)010⟨0065:rhtfaf⟩2.0.co;2

Wilks, D. S. (2011). *Statistical methods in the atmospheric sciences.* Amsterdam; Boston: Elsevier Academic Press.

Woollings, T., Hannachi, A., & Hoskins, B. (2010). Variability of the North Atlantic eddy-driven jet stream. *Q. J. R. Meteorol. Soc.*, *136*(649), 856–868. doi: 10.1002/qj.625

Wu, S., Mickley, L. J., Leibensperger, E. M., Jacob, D. J., Rind, D., & Streets, D. G. (2008). Effects of 2000–2050 global change on ozone air quality in the United States. *J. Geophys. Res.*, *113*(D6). doi: 10.1029/2007JD008917

Zhang, Y., & Wang, Y. (2016). Climate-driven ground-level ozone extreme in the fall over the southeast United States. *Proc. Natl. Acad. Sci. U.S.A.*, *113*(36), 10025–10030. doi: 10.1073/pnas.1602563113

Zhao, S., Pappin, A. J., Morteza Mesbah, S., Joyce Zhang, J. Y., MacDonald, N. L., & Hakami, A. (2013). Adjoint estimation of ozone climate penalties. *Geophys. Res. Lett.*, *40*(20), 5559–5563. doi: 10.1002/2013GL057623

Zhao, Z., & Wang, Y. (2017). Influence of the West Pacific subtropical high on surface ozone daily variability in summertime over eastern China. *Atmos. Environ.*, *170*, 197–204. doi: 10.1016/j.atmosenv.2017.09.024

Zhu, J., & Liang, X.-Z. (2013). Impacts of the Bermuda High on regional climate and ozone over the United States. *J. Clim.*, *26*(3), 1018–1032. doi: 10.1175/jcli-d-12-00168.1

Zhuang, J. (2018). *Jiaweizhuang/xesmf: v0.1.1.* Zenodo. doi: https://doi.org/10.5281/ZENODO.1134366

Zwiers, F. W., & von Storch, H. (1995). Taking serial correlation into account in tests of the mean. *J. Clim.*, *8*(2), 336–351. doi: 10.1175/1520-0442(1995)008⟨0336:tsciai⟩2.0.co;2

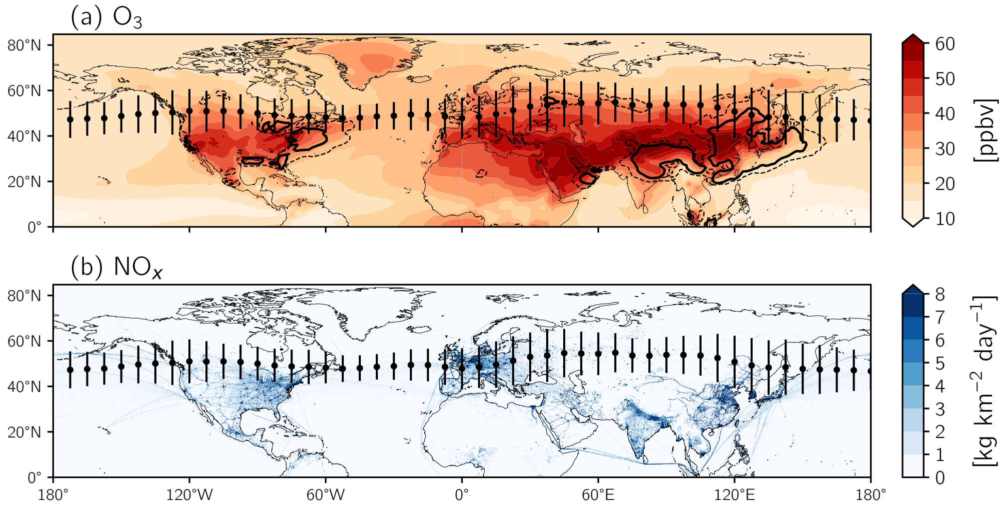

Figure 1. (a) Time-averaged O_3 from the surface-level of the GMI CTM (colored shading). Black contours indicate O_3 variability (standard deviation): thin dashed contour, 8 ppbv; thick contour, 10 ppbv. (b) Time-averaged anthropogenic NO_x emissions from EDGAR. Scatter points and error bars in (a-b) specify the mean position and variability of the jet stream, respectively.

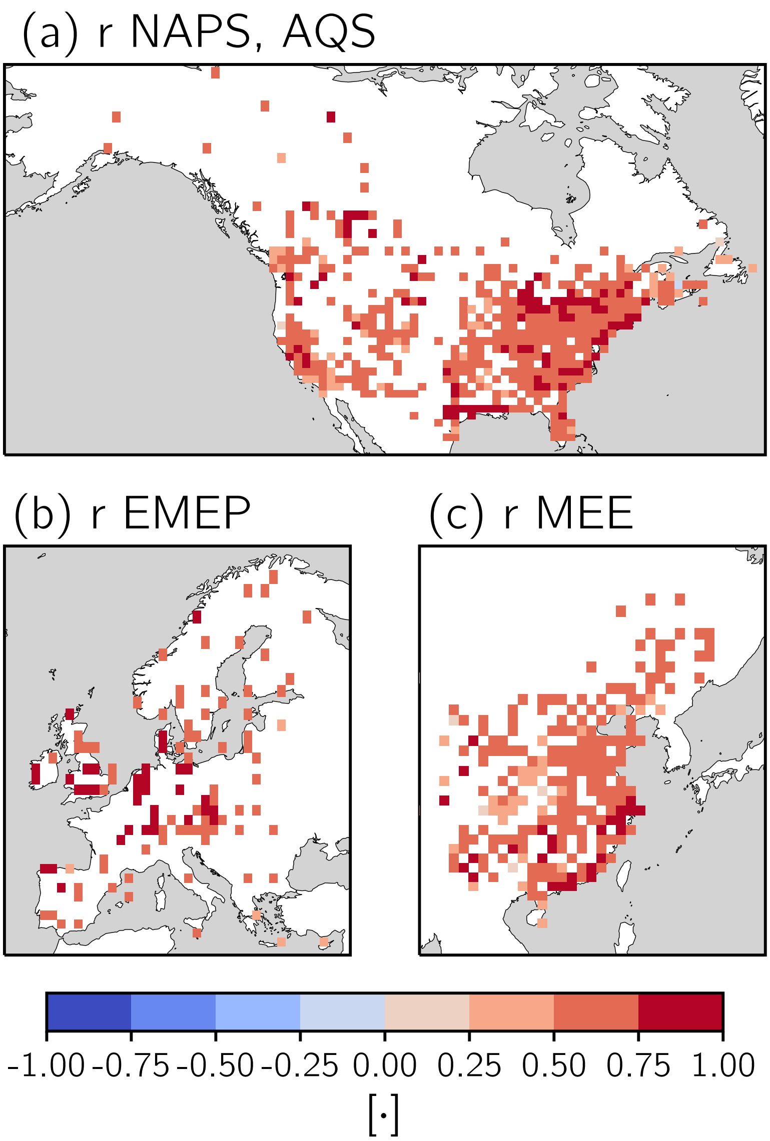

Figure 2. The correlation coefficient (r) calculated between modeled O_3 from the GMI CTM and observed O_3 for model grid cells containing *in-situ* monitor(s). The networks in (a) North America, (b) Europe, and (c) China from which monitor-based observations have been derived are indicted in the subplots' titles. If there is $>$ 1 monitor in a grid cell, all O_3 observations are averaged to produce a grid cell average prior to computing r.

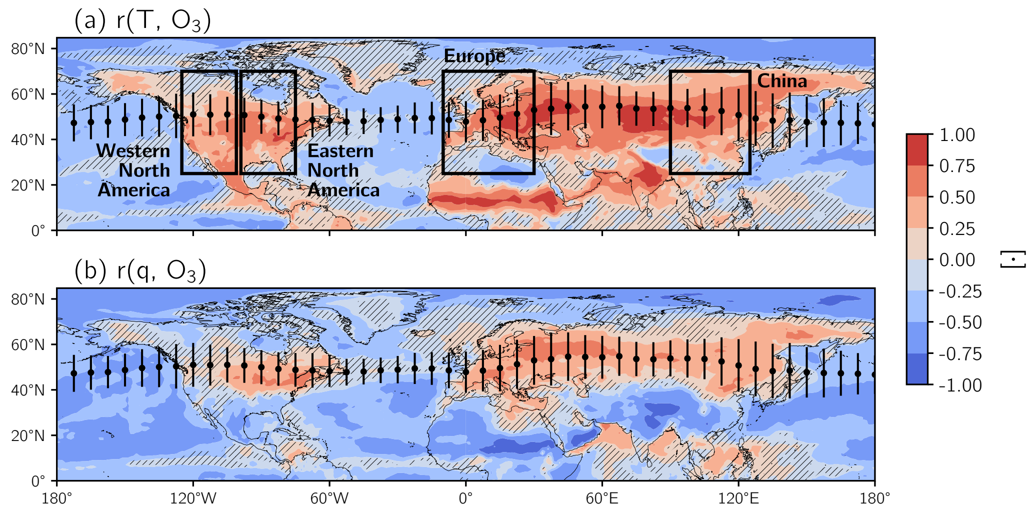

Figure 3. (a) The correlation coefficient calculated between O_3 from the GMI CTM and MERRA-2 temperature, $r(T, O_3)$. Hatching denotes regions where the correlation is insignificant, determined using moving block bootstrap resampling to estimate the 95% confidence interval. (b) Same as (a) but for the correlation coefficient calculated between between O_3 and MERRA-2 specific humidity, $r(q, O_3)$. Scatter points and error bars in (a-b) specify the mean position and variability of the jet stream, respectively. Black boxes in (a) outline the regions over which zonal averages were performed in Figure 4.

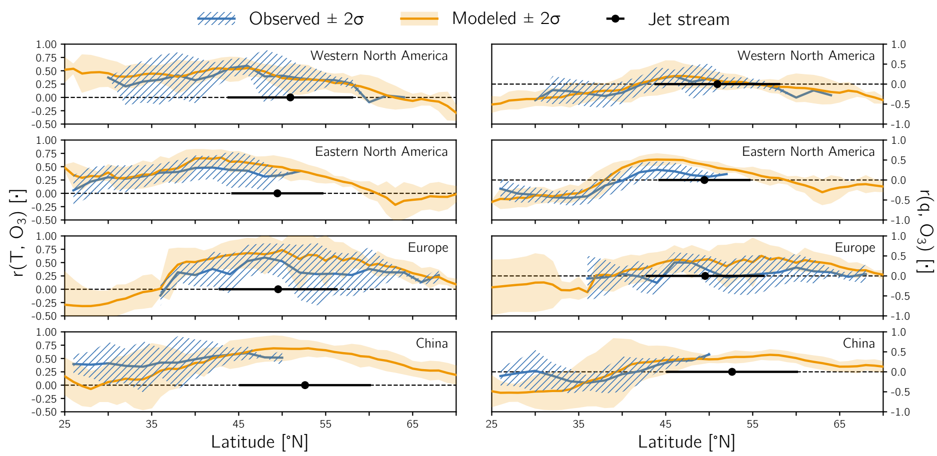

Figure 4. Zonally-averaged observed and modeled (left) $r(T, O_3)$ and (right) $r(q, O_3)$ in four regions: Western North America ($125° - 100°$W), Eastern North America ($100° - 65°$W), Europe ($10°$W$-30°$E), and East Asia ($90 - 125°$E). These regions are also outlined in Figure 3a. Zonally-averaged modeled relationships consider only grid cells over land, and the observed relationships are binned by latitude to compute the zonal average. The dashed grey lines delineate positive from negative values of the O_3-meteorology relationships, and the scatter points and error bars corresponding to the jet and its variability are the same as in Figure 1 but averaged over each region.

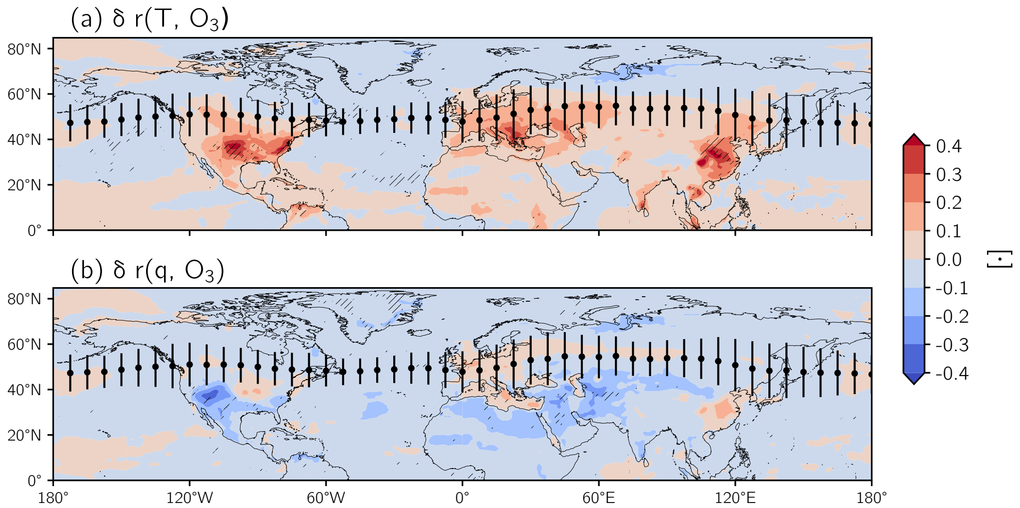

Figure 5. The difference in (a) $r(T, O_3)$ and (b) $r(q, O_3)$ calculated between the control and transport-only CTM simulations. Hatching indicates regions with significant $r(T, O_3)$ or $r(q, O_3)$ in the control simulation that became insignificant in the transport-only simulation. Scatter points and error bars in (a-b) specify the mean position and variability of the jet stream, respectively.

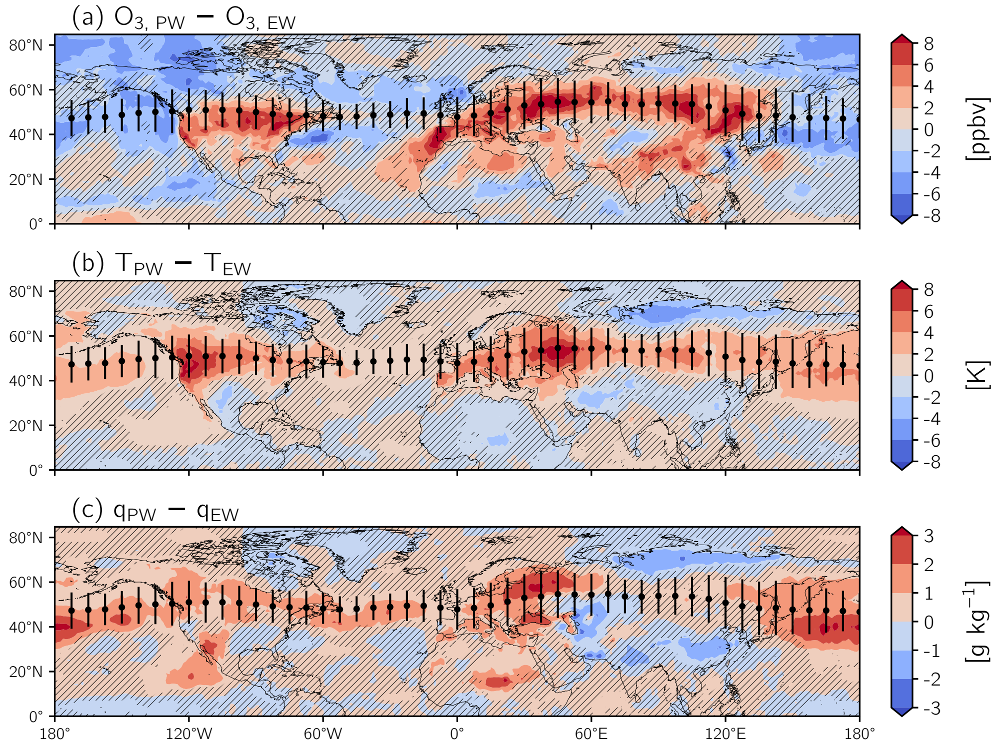

Figure 6. The difference in composites of (a) O_3, (b) temperature, and (c) specific humidity on days when the jet is in a poleward (PW) and equatorward (EW) position. Composites are formed for the PW (EW) case by determining the value of each field in (a-c) averaged over all days when the position of the jet stream (ϕ_{jet}) exceeds the 70th (is less than the 30th) percentile for each longitude. Hatching indicates regions where the correlation between each field and the distance from the jet is insignificant. The distance from the jet, $\phi - \phi_{jet}$, is defined as the difference, in degrees, between the local latitude and the latitude of the jet. Scatter points and error bars in (a-c) specify the mean position and variability of the jet stream, respectively.

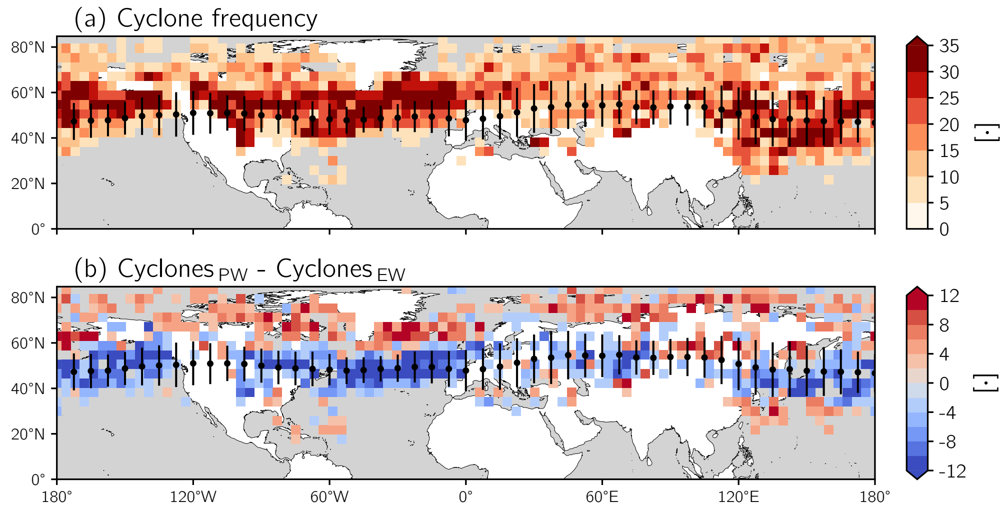

Figure 7. (a) Total number of cyclones detected by MCMS on sub-daily (six-hourly) time scales binned to a $\sim 4^\circ \times 4^\circ$ grid. (b) The difference in the total number of cyclones calculated between days when the jet is in a poleward (PW) and equatorward (EW) position. Scatter points and error bars in (a-b) specify the mean position and variability of the jet stream, respectively.

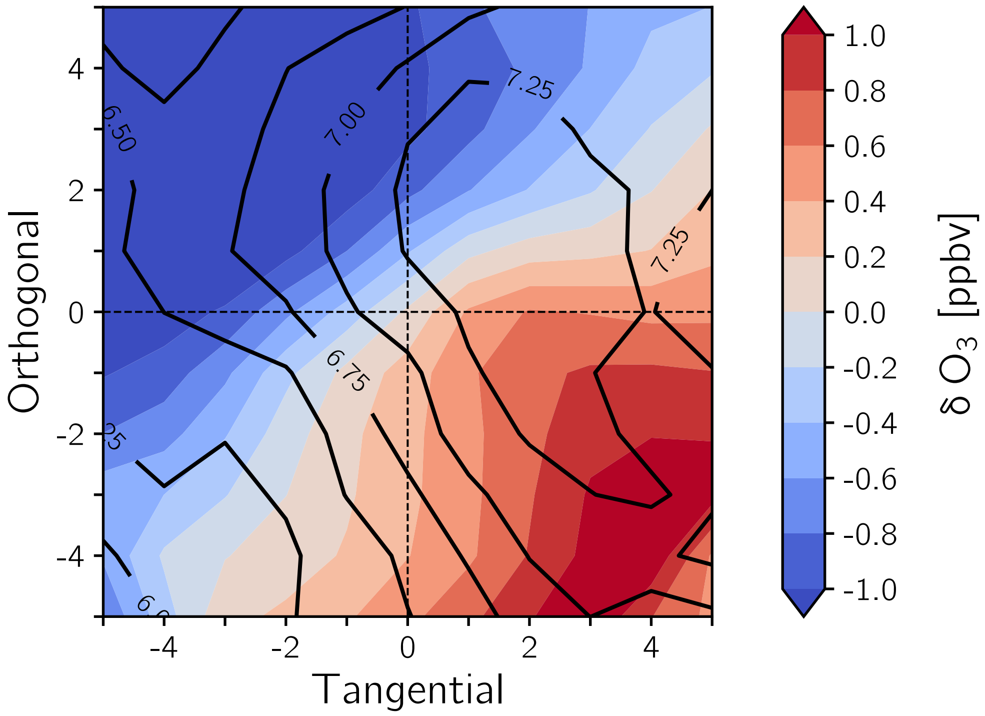

Figure 8. The average O_3 anomaly (colored shading) and standard deviation of the anomalies (solid black contours) within five grid cells ($\sim$ 5°) of the position of the cyclones. From the cyclones shown in Figure 7, we only consider cyclones occurring over land and detected for $\geq$ 2 time steps and subsequently rotate the cyclones following the direction of their propogation such that they move to the right of the figure. Dashed black lines divide the cyclone composites into quadrants.

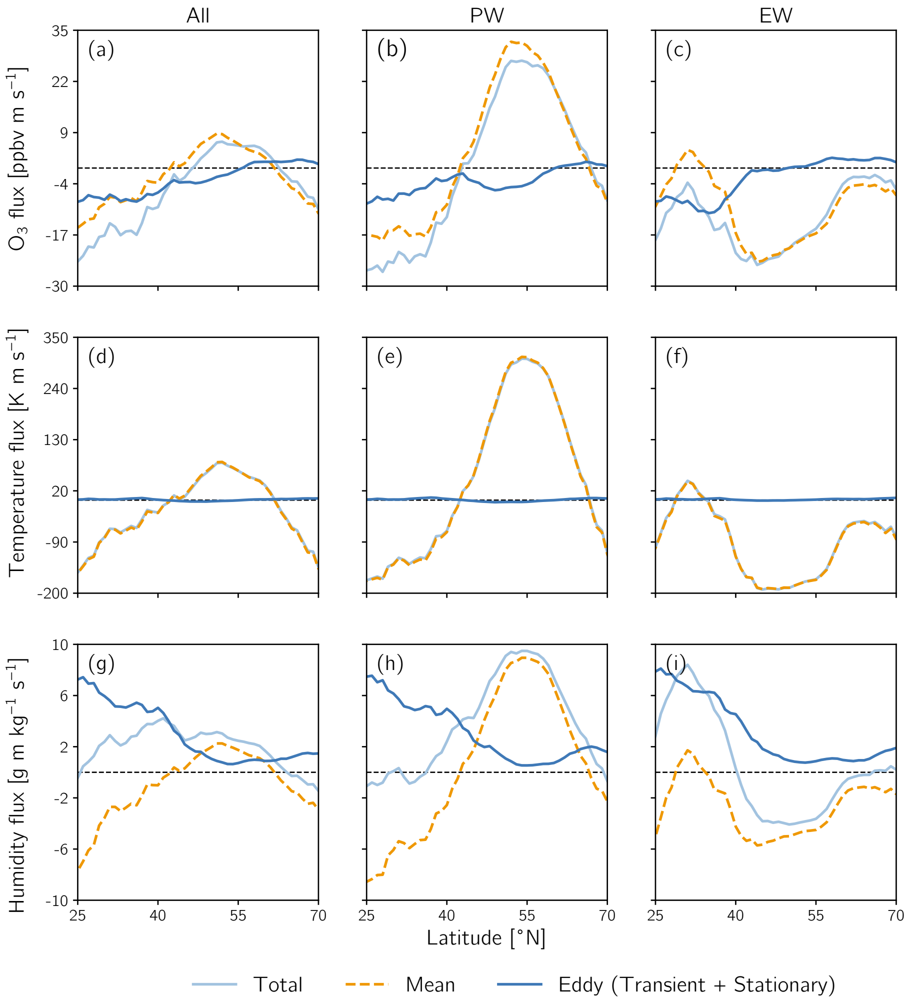

Figure 9. The zonally-averaged total flux of (a-c) O_3, (d-f) temperature, and (g-i) specific humidity and the contributions from the mean and eddy components. Calculations of the total flux and its components are done for all days (first column; a, d, g), days when the jet is in a PW position (second column; b, e, h), and days when the jet is in a EW position (third column; c, f, i).

Supporting Information for "Surface ozone-meteorology relationships: Spatial variations and the role of the jet stream"

Gaige Hunter Kerr[1], Darryn W. Waugh[2,3], Stephen D. Steenrod[3,4], Sarah A. Strode[3,4], and Susan E. Strahan[3,4]

[1]Department of Earth and Planetary Sciences, Johns Hopkins University, Baltimore, Maryland, USA

[2]School of Mathematics and Statistics, University of New South Wales, Sydney, New South Wales, Australia

[3]NASA Goddard Space Flight Center, Greenbelt, Maryland, USA

[4]Universities Space Research Association, GESTAR, Columbia, Maryland, USA

Contents of this file

1. Text S1 to S2
2. Figures S1 to S3

Text S1: Planetary boundary layer (PBL) dynamics

Variations in the height of the PBL ($PBLH$) could connect the jet to surface-level O_3, temperature, and humidity. $PBLH$ determines vertical mixing and the dilution of surface-level pollutants (Dawson et al., 2007) and responds directly to the flux of heat into the PBL. Previous studies have used both $PBLH$ and mixing height to assess the impact of PBL dynamics on surface-level pollutants (e.g., Jacob & Winner, 2009; Reddy & Pfister, 2016), and here we use daily mean MERRA-2 $PBLH$, detailed in Section 2.3 of the main text.

An analysis of the (PW - EW) composites shows that the daily north-south movement of the jet stream is not significantly associated with $PBLH$ variability over a majority of the continental regions of the Northern Hemisphere (Figures S3a, S4a). Over the oceans, northward movement of the jet stream tends to be associated with a more shallow boundary layer; but, in general, there is a no consistent sign associated with the variability of the jet with $PBLH$ (Figure S3a, S4a). This result is robust whether daily mean $PBLH$ is used as we have here, or if the jet-$PBLH$ relationship is derived using $PBLH$ averaged over subsets of the day (e.g., daytime, afternoon).

Although there is no jet-$PBLH$ relationship, it is possible that $PBLH$ may influence ozone independent of the jet stream. To examine this we evaluate the correlation between $PBLH$ and O_3. The sign of this correlation is varied, and its strength is largely insignificant across the mid-latitudes (not shown). There are some regions where $r(PBLH, O_3)$ is significant positively, but this implies that a deeper PBL results in higher O_3, which goes against simple dilution arguments. These findings agree with other studies: Jacob and Winner (2009) pointed out that the effect of mixing depth on O_3 is weak or variable (while the effect of mixing depth on $PM_{2.5}$ is consistently negative).

Text S2: Near-surface winds

Another possible mechanism for the jet-O_3 relationship is changes in near-surface flow. We form additional (PW - EW) composites but for near-surface eastward (U_{10}) and northward (V_{10}) winds (Figure S3b-c). In a $\sim 20°$ latitudinal band north (south) of $\overline{\phi_{jet}}$, the poleward (equatorward) movement of the jet significantly increases (decreases) U_{10} by up to 4 m/s (Figure S3a). Figure S3b asserts that V_{10} increases by up to 3 m/s as the jet migrates north throughout the mid-latitudes. It is worth noting the largest areal extent of changes (both increases and decreases) in U_{10} are centered over the oceans, while increases in V_{10} occur throughout the mid-latitudes over both land and oceans (Figure S3b-c).

The spatial structure of the change in V_{10} is qualitatively similar to the impact of the jet stream on other fields (e.g., O_3, temperature, and humidity in Figure 6 of the main text), but we note that there are some marine regions the windward side of continents where V_{10} has a negative relationship with the jet stream. Outside of the mid-latitudes the sign and significance of the relationship of the jet with U_{10} and V_{10} is varied.

The composites in Figure S3b-c are less meaningful unless placed in the context of the time-averaged direction and magnitude of U_{10} and V_{10}, and we next discuss this. The time-averaged U_{10} is generally positive (eastward) over both land and ocean in the mid-latitudes ($40 - 60°$N) with a speed of $\sim$ 1 m/s, while V_{10} in this latitudinal band is varied and generally weak ($-0.5 < V_{10} < 0.5$ m/s) (not shown). Thus, given the average speed and magnitude of U_{10} and V_{10}, the differences in V_{10} over land given the meridional vacillation of the jet (Figure S3c) represent much larger percentage changes than the jet-associated changes in U_{10}.

We also analyze the correlation between and U_{10} or V_{10} (Figure S3b-c). This analysis further supports that the ϕ_{jet} is linked to changes in near-surface flow in the mid-latitudes and that V_{10} strengthens as the jet migrates poleward.

We investigated the relationship among ϕ_{jet} and the total near-surface wind ($|U_{10}|$), a proxy for stagnation (not shown). Differences in $|U_{10}|$ between days with a poleward- versus equatorward-shifted jet were weak and variable in sign, and the correlation was insignificant across virtually the entire hemisphere. As we did with $PBLH$, we considered the impact that $|U_{10}|$ has on O_3 independent of the jet, as weak flow can inhibit the ventilation of the PBL (Mickley, 2004). We found that O_3 and $|U_{10}|$ were generally anticorrelated in the mid-latitudes; however, these correlations were weak and insignificant. There were also parts of the mid-latitudes with positive correlations between O_3 and $|U_{10}|$, implying that higher wind speeds and therefore increased ventilation are associated with higher concentrations of O_3.

References

Dawson, J. P., Adams, P. J., & Pandis, S. N. (2007). Sensitivity of ozone to summertime climate in the eastern USA: A modeling case study. *Atmos. Environ.*, *41*(7), 1494–1511. doi: 10.1016/j.atmosenv.2006.10.033

Jacob, D. J., & Winner, D. A. (2009). Effect of climate change on air quality. *Atmos. Environ.*, *43*(1), 51–63. doi: 10.1016/j.atmosenv.2008.09.051

Mickley, L. J. (2004). Effects of future climate change on regional air pollution episodes in the United States. *Geophys. Res. Lett.*, *31*(24). doi: 10.1029/2004GL021216

Reddy, P. J., & Pfister, G. G. (2016). Meteorological factors contributing to the interannual variability of midsummer surface ozone in Colorado, Utah, and other western U.S. states. *J. Geophys. Res.*, *121*(5), 2434–2456. doi: 10.1002/2015JD023840

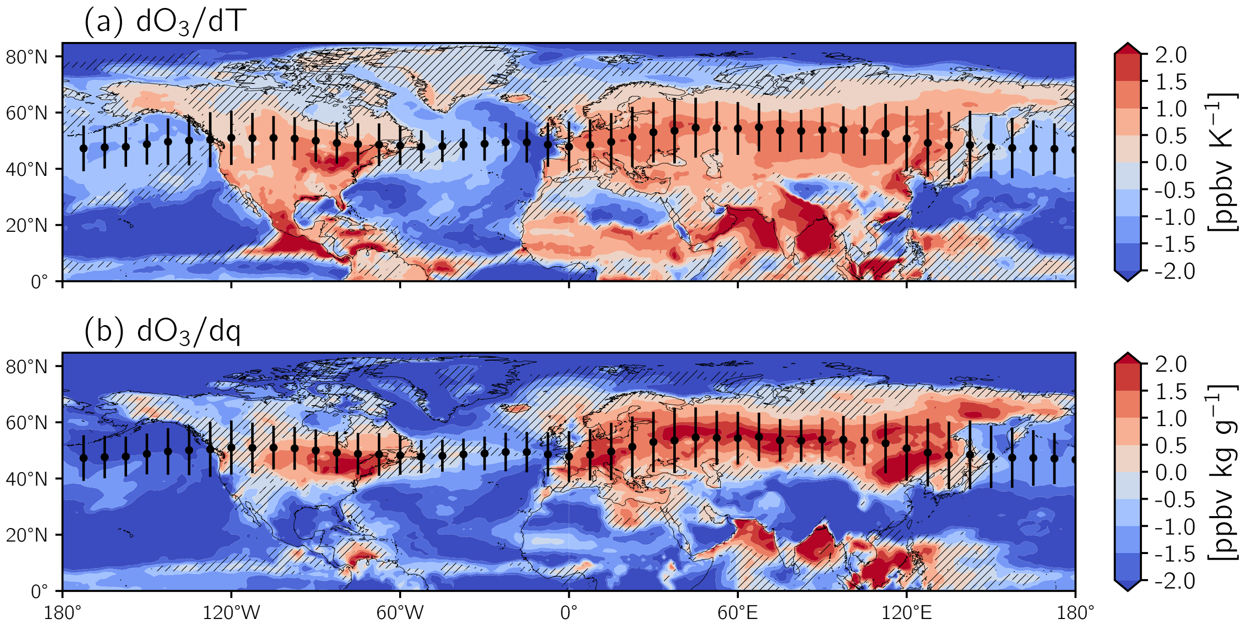

Figure S1. (a) The slope of the ordinary least squares (OLS) regression of O_3 versus temperature, dO_3/dT. Hatching denotes regions where the correlation between O_3 and temperature is insignificant, determined using moving block bootstrap resampling to estimate the 95% confidence interval. (b) Same as (a) but for O_3 versus specific humidity, dO_3/dq, with hatching showing insignificant correlation between O_3 and specific humidity. Scatter points and error bars are identical in (a-b) and show the mean latitude of the eddy-driven jet and its variability.

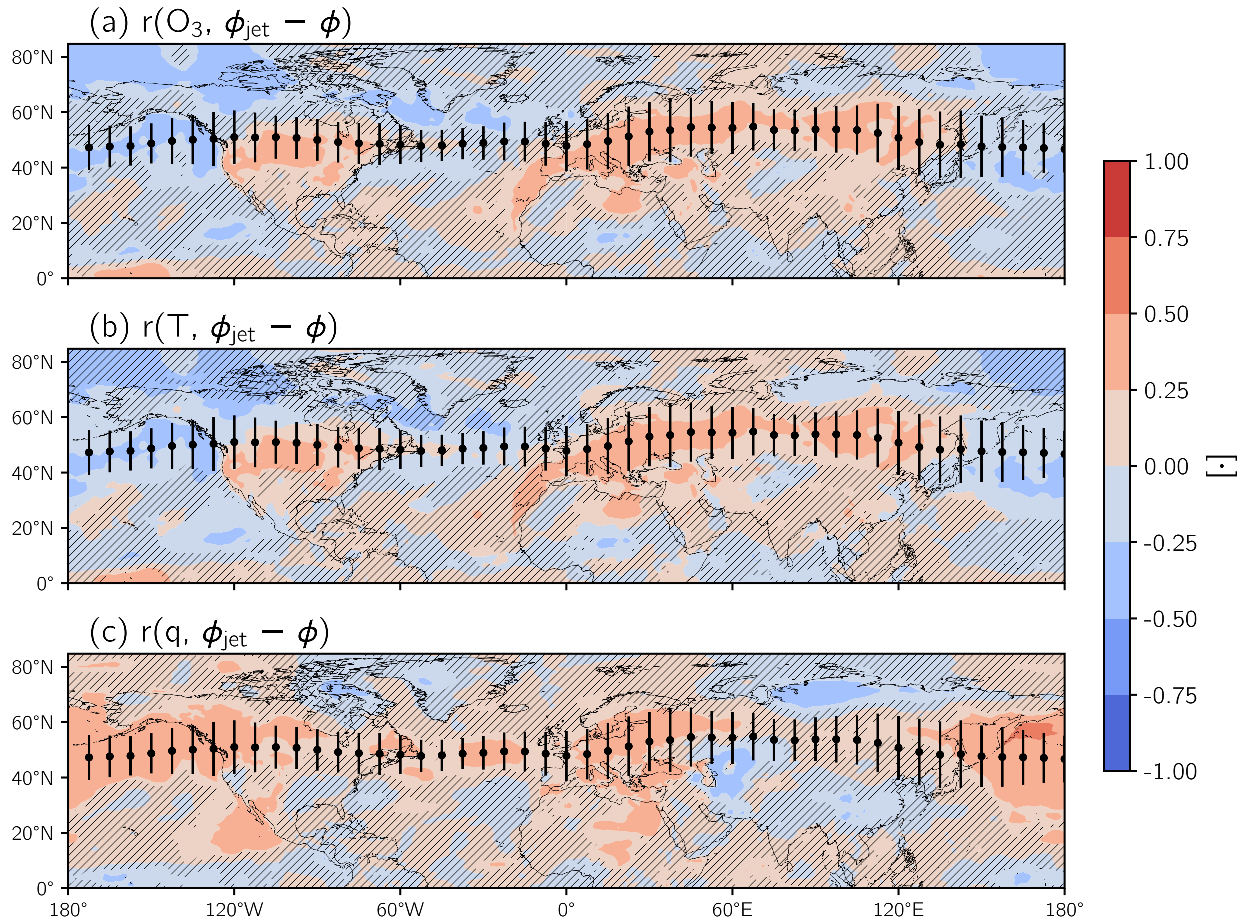

Figure S2. Colored shading shows the correlation coefficient (r) calculated between distance from the eddy-driven jet and (a) O_3, (b) temperature (T), and (c) specific humidity (q). Hatching is the same as in Figure 6, and scatterpoints, and error bars are the same as in Figure 3.

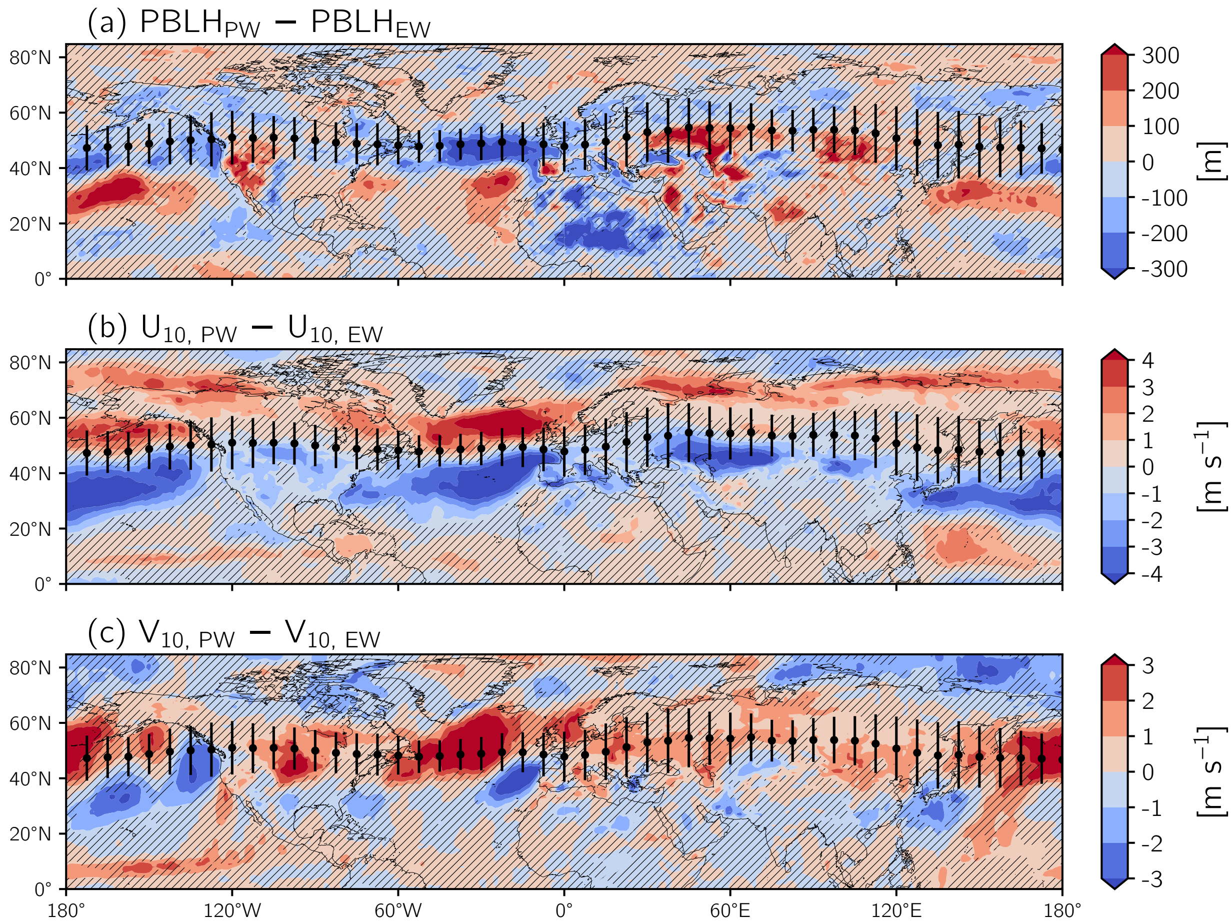

Figure S3. Same as Figure 6 in the main text but for (a) $PBLH$, (b) U_{10}, and (c) V_{10}.

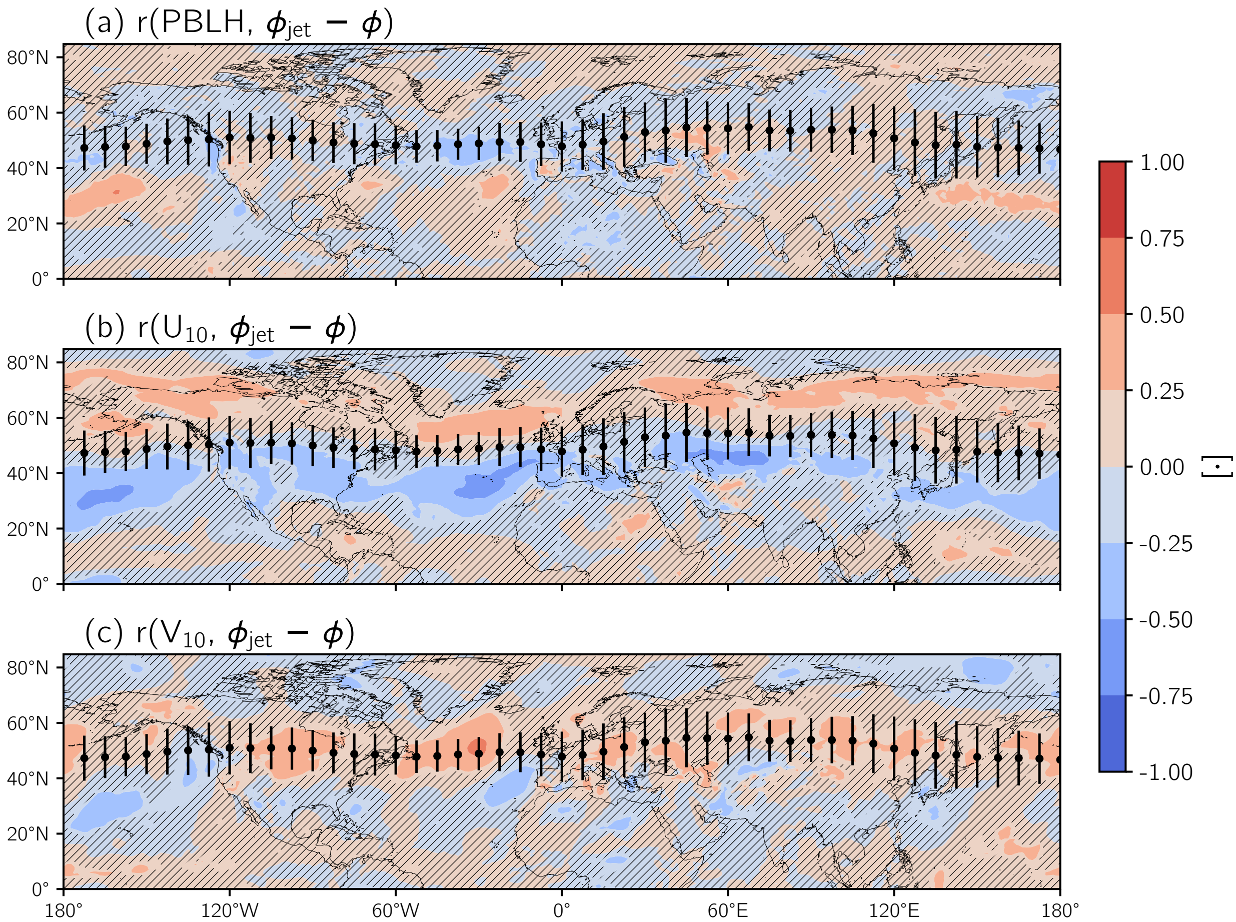

Figure S4. Same as Figure S2 but for (a) $PBLH$, (b) U_{10}, and (c) V_{10}.